Cr(VI) reduction, electricity production, and microbial resistance variation in paddy soil under microbial fuel cell operation

Huan Niu[b], Can Wang[a]*, Xia Luo[b], Peihan Li[b], Hang Qiu[b], Liyue Jiang[b], Subati Maimaitiaili[b], Minghui Wu[b], Fei Xu[c], Heng Xu[c]

a State Key Laboratory of Geohazard Prevention and Geoenvironment Protection, College of Ecology and Environment, Chengdu University of Technology, Chengdu, 610059, China

b Sichuan Engineering Research Center for Biomimetic Synthesis of Natural Drugs, School of Life Science and Engineering, Southwest Jiaotong University, Chengdu, 610031, Sichuan, P.R. China

c Key Laboratory of Bio-Resource and Eco-Environment of Ministry of Education, College of Life Sciences, Sichuan University, Chengdu 610065, Sichuan, PR China

* Corresponding at No. 111 Second Ring Road, Chengdu, Sichuan, 610031, China. Tel: + 86 18728156952

E-mail: wangcan@swjtu.edu.cn (Can Wang)

1   **Abstract figure:**

"physio-bio" adsorption and reduction of Cr(VI) under bioelectrochemical driving
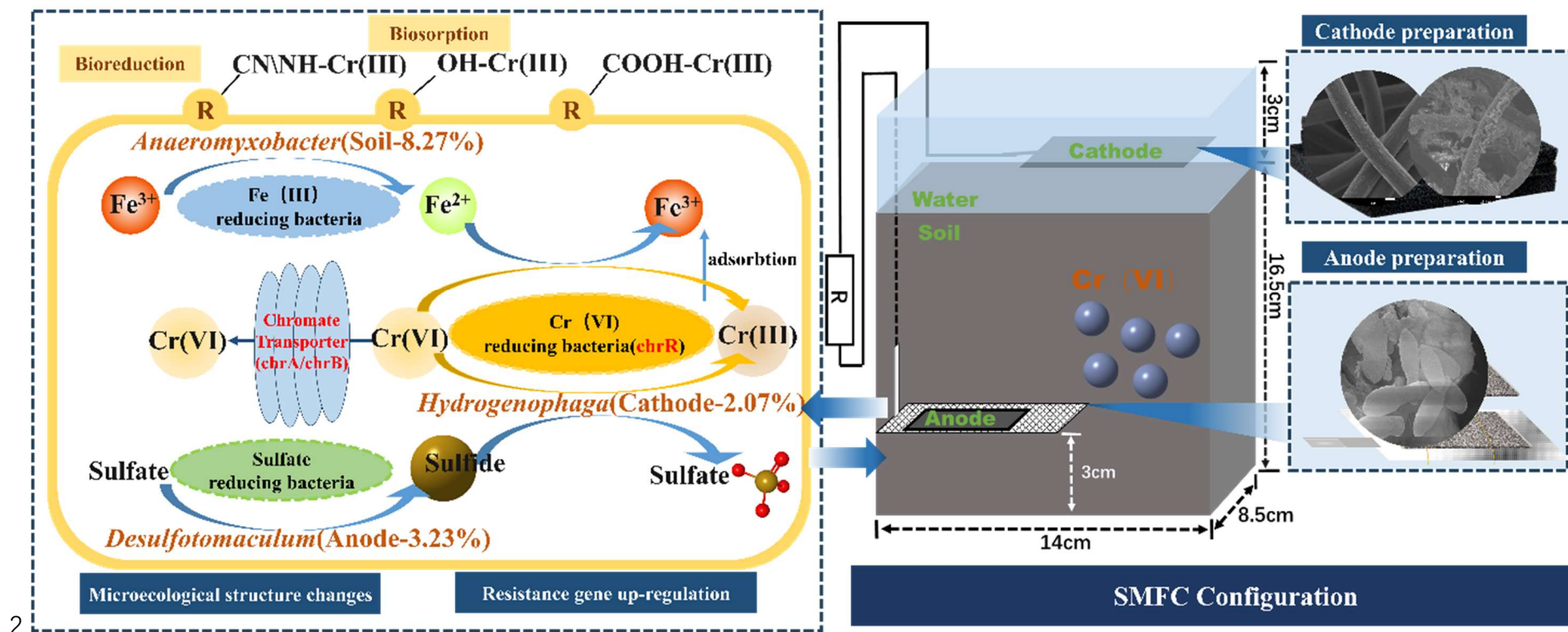
Abstract: Microbial fuel cell (MFC) is an efficient in-situ approach to combat pollutants and generate electricity. This study constructed a soil MFC (SMFC) to reduce Cr(VI) in paddy soil and investigate its influence on microbial community and microbial resistance characteristics. Fe_3O_4 nanoparticle as the cathodic catalyst effectively boosted power generation (0.97 V, 102.00 mW/m^2), whose porous structure and reducibility also contributed to Cr reduction and immobilization. After 30 days, 93.67% of Cr(VI) was eliminated. The bioavailable Cr decreased by 97.44% while the residual form increased by 88.89%. SMFC operation greatly changed soil enzymatic activity and microbial structure, with exoelectrogens like *Desulfotomaculum* (3.32% in anode) and Cr(VI)-reducing bacteria like *Hydrogenophaga* (2.07% in cathode) more than 1000 folds of soil. In particular, SMFC operation significantly enhanced heavy metal resistance genes (HRGs) abundance. Among them, *chrA, chrB,* and *chrR* increased by 99.54~3314.34% in SMFC anode, probably attributed to the enrichment of potential tolerators like *Acinetobacter, Limnohabitans,* and *Desulfotomaculum*. These key taxa were positively correlated with HRGs but negatively correlated with pH, EC, and Cr(VI), which could have driven Cr(VI) reduction. This study provided novel evidence for bioelectrochemical system application in contaminated paddy soil, which could be a potential approach for environmental remediation and detoxification.

Keywords: Chromium; Microbial fuel cell; Microbial response; Metal resistance

Nomenclature	
SMFC	Soil microbial fuel cell
HRGs	Heavy metal resistance genes
HMs	Heavy metals
HGT	Horizontal gene transfer
EAB	Electrochemical active bacteria
GF	Graphite felt
ORR	Oxygen reduction reaction
WCV	Working circuit voltage
OCV	Open circuit voltage
ARGs	Antibiotic resistance genes
CMFC-A	Anode of the closed circuit group
OMFC-A	Anode of the open circuit group
CMFC-C	Cathode of the closed circuit group
OMFC-C	Cathode of the open circuit group
CMFC-S	Soil of the closed circuit group
OMFC-S	Soil of the open circuit group
NMFC-S	Soil of the non-electrode control group

1. Introduction

Chromium (Cr) is a main toxic heavy metal (HM), that enters the environment mainly due to its wide

use in electroplating, tanning, and other industries (Coetzee et al., 2020). Mineral-sourced phosphate

fertilizer also contains high-level Cr, promoting its spreading, migration and accumulation in soil and

underground water (Chen et al., 2022a). The persistence and toxicity of HMs create permanent and

selective stress on environmental microbes. Under the toxic stress, microorganisms have deployed

various strategies, including active efflux of the toxic from the microbial cell, regulation of targets, and

enzymatic modification of the toxic, presenting as elevation of heavy metal resistance gene (HRG) and

tolerant microbe (Van Hoek et al., 2011). Even a sub-dose of Cr (especially the Cr(VI) state) can promote

plasmid-mediated horizontal gene transfer (HGT) (Zhang et al., 2018), causing HRG enrichment,

threatening environmental safety (Guo et al., 2021; Wang et al., 2020a; Wang et al., 2023b). Meanwhile,

due to the co-selection effect, the long-term existence of HMs also causes the enrichment of antibiotic-

32   resistant bacteria (ARB), further increasing the resistance gene spreading risk in the environment (Men

33   et al., 2018). Such a threat could be more fierce under the coexistence of HMs and antibiotics (Ashbolt

34   Nicholas et al., 2013). Hence, the enrichment of HRGs and ARB under Cr exposure has become an

35   emerging concern.

36   Common remediation methods for Cr-influenced soil include chemical reduction and leaching

37   (Cong et al., 2022), electrokinetic remediation (Morales-Benítez et al., 2023), and phytoaccumulation

38   (Yaashikaa et al., 2022), which convert Cr(VI) into insoluble and low toxic forms (e.g., Cr(III)) by

39   adsorption, ion exchange, and redox (Rani et al., 2022). Among them, the microbial approach using

40   functional microbes is commonly used for the continuous treatment of soil-groundwater, which has a

41   low cost without side effects (Fan et al., 2023). For example, *Comamonas testosteroni* bacterial strains

42   are used to degrade hexachlorobenzene and *Acinetobacter calcoaceticus GSN3* strain to degrade phenol

43   (Dimova et al., 2022; Irankhah et al., 2019). However, pollutants can be tightly adsorbed by soil particles

44   and persistently remain (Wang et al., 2023c). The complex soil constituents and competition of

45   indigenous microorganisms inhibit the colonization and development of functional microbes and limit

46   their effectiveness (Guo et al., 2021).

47   Microbial fuel cell (MFC) technology can transform or immobilize HMs and generate electricity

48   utilizing electrochemical active bacteria (EABs) (Gupta et al., 2023; Chen et al., 2022b), which have

49   been used in sediment or soil to treat HMs and organics and monitor environmental toxicity (Li et al.,

50   2023b). For example, soil microbial fuel cells can mitigate the accumulation of heavy metals in rice and

51   promote the removal of atrazine in the soil (Gustave et al., 2020; Farkas et al., 2024). At present, soil

52   MFC (SMFC) has been used for pollution control, focusing on pollutant content and forms as well as the

electrochemical properties (Hamdan and Salam, 2023; Liu et al., 2023a). There is a lack of systematic research about the MFC effect on soil microbial community structure shifting and resistance characteristics, especially under the HMs contamination circumstance.

In this study, an SMFC was constructed to remediate Cr(VI) contaminated paddy soil. EABs were pre-loaded on the SMFC anode to promote electricity production and Cr transformation. Ferroferric oxide (Fe_3O_4) nanoparticles, which can reduce and fix Cr(VI) directly, were used as a catalyst for cathodic oxygen reduction reaction (ORR) to improve SMFC performance due to its catalytic effect, non-toxicity, cost-effectiveness, and free of secondary pollution (Liu et al., 2023b). During operation, Cr(VI) was simultaneously reduced and immobilized by bio-physical adsorption and electrochemical-microbial reduction. The Cr(VI) reduction mechanism and the analysis of microbial community structure shaping and HRG variation were comprehensively studied. For the first time, SMFC-driven Cr(VI) reduction was associated with microbial resistance, which evolved along with microbial adaptation and development. This study not only provides a reference for the microbial remediation of polluted soil but also improves the practical field application of MFC. The method can be used for in-situ contaminant treatment in various environments, such as aquaculture ponds, inland lakes, and wetlands.

2.   Materials and Methods

2.1. Chemicals

All the chemicals and reagents were analytical grade or premium pure from Kelong Chemical Reagent Factory, Chengdu, China.

2.2 Construction of SMFC

2.2.1 Soil

Paddy soil from Jintang County, Chengdu, China (30°74' N, 104°59' W) was collected and used to construct SMFC. The soil has organic matter, organic carbon, and total nitrogen of 8.84±0.02%, 1.74±0.01%, and 321.67±1.25 mg/kg, respectively. Referring to the previous studies and the Chinese Soil Environmental Quality Standard (GB15618-2018), 120.00 mg/kg potassium dichromate was added to the soil and a final Cr(VI) concentration of 118.80 mg/kg was achieved before use (Liu et al., 2020; Mandal et al., 2017; Li et al., 2024).

2.2.2 Electrodes Preparation

Aluminum foam ($66.00 \times 54.00 \times 5.00$ mm, porosity 60.00-80.00%, bulk density 0.50-1.10 g/cm^3) (SANZHENG Metal material, Chengdu, China) was used as anode. The anode microflora was derived from municipal sludge (Chengdu Sixth Sewage Treatment Plant, China) after acclimating with 100.00 mg/L Cr(VI). Before assembling, the aluminum foam was cultivated in the anode microflora for 2 weeks. Then the anode was tied to titanium mesh tightly with titanium wire. Graphite felt (GF) ($100.00 \times 50.00 \times 3.00$ mm, bulk density 0.10-0.15 g/cm^3) was used as the cathode (Table S1). Before use, it was cleaned, dried, and loaded with Fe_3O_4 as the ORR catalyst, as detailed in section 1 of the supplementary material. For characterization, we utilized a scanning electron microscope (SEM) to examine the structure and morphology of the electrode surface. In addition, we performed X-ray photoelectron spectroscopy (XPS) and energy dispersive spectroscopy (EDS) to analyze the valence state and element composition. The phase composition was determined using an X-ray diffractometer (XRD).

92 2.2.3 SMFC construction

93 A plastic box (140.00×85.00×165.00 mm) was used as the SMFC reactor, with 1.50 kg air-dried soil and

94 overlying water of 3.00 cm to simulate the flooded state during rice planting. The cathode was floated

95 on the water surface while the anode was buried (about 3.00 cm from the bottom). The cathode and anode

96 were connected to a 2000 Ω resistor using titanium wire. The water level was kept constant by daily

97 replenishment (Fig. S1).

2.3 Design and Operation

99 Three treatments were set up as shown in Fig. S1, and three parallels were set for each group. NMFC:

100 The control group with no electrode, only contains an equal amount of overlying water and paddy soil.

101 OMFC: The open circuit group with disconnected electrodes and equal amounts of overlying water and

102 paddy soil. CMFC: The complete closed-circuit SMFC capable of producing electricity, with electrodes

103 connected by a 2000 Ω resistor, and equal amounts of overlying water and paddy soil.

104 The experiments were conducted at 25°C. A Raspberry Pi data acquisition system (ARMv7

105 architecture) was connected at both ends of the resistor of CMFC to monitor the voltage. A multimeter

106 was used for verification. The detailed code information can be found in section 2 of the supplementary

107 material.

108 Soil and water samples were taken every 5 days until day 35, and the operation continued for another

109 10 days until day 45 (Specific sampling details are given in the supplementary file). The electrochemical

110 properties of the SMFC including the polarization curve and power density curve were tested using an

111 electrochemical workstation on days 15 and 30 (Ch660e, Shanghai Chenhua Instrument Co., Ltd.,

112 Shanghai, China) (Chen et al., 2022b).

2.4 Cr Migration and Transformation

To determine total Cr, 0.50 g soil was subjected to acid digestion (HCl-HNO$_3$-HClO$_4$) before measurement using flame atomic absorption spectrometry (FAAS) (PinAAcle 900T AA Spectrometer, PerkinElmer, America). To determine Cr speciation, BCR sequential extraction was applied to divide Cr into HOAc extractable, reducible, oxidizable, and residual fractions with mobility and availability from high to low (Wang et al., 2020a). Also, Cr(VI) concentration in overlying water was determined by a spectrophotometer at 540 nm, while Cr(VI) in soil was determined using FAAS after alkaline digestion (Fan et al., 2021). Duplicates, method blanks, and standard reference materials were used for quality control. Cr recovery in standard reference materials was 92.00~108.00%.

2.5 Microbial response during operation

2.5.1 Soil biochemical response

Soil dehydrogenase (DHA) activity was measured using 2, 3, 5-triphenyl tetrazolium chloride (TTC) method. Urease activity was determined by the phenol sodium hypochlorite colorimetric assay. Invertase activity was determined by the 3, 5-dinitro salicylic acid colorimetric assay. The acid phosphatase (ACP) activity was determined by the p-nitrophenyl disodium phosphate colorimetric assay (Wang et al., 2019; Wang et al., 2017).

2.5.2 Microbial community structure

The microbial community structure of the electrodes and soil was determined by high-throughput sequencing (Faust and Raes, 2012; Deng et al., 2012; Bokulich et al., 2018). Majorbio (Shanghai, China) performed 16S rRNA gene sequencing using the Illumina HiSeq platform. 0.50 g of fresh homogenized samples were used to extract the total bacterial DNA with a universal DNA Kit (Omega Biotek Inc.,

134   USA). After amplification and purification, the V3-V4 hypervariable regions of the bacterial 16S rRNA

135   gene were amplified with primer pairs 338F and 806R. After sequencing, the operational taxonomic units

136   (OTUs) with a 97.00% similarity cutoff were clustered using UPARSE version 7.1, and chimeric

137   sequences were identified and removed. The taxonomy of each OTU representative sequence was

138   analyzed by RDP Classifier version 2.2 against the 16S rRNA database using a confidence threshold of

139   0.7. The alpha diversity, beta diversity, microbial community structure change, and environmental factor

140   correlation analysis were conducted. (Wang et al., 2023a)

141   2.5.3 HRG Fluctuation

142   Microbial DNA Rapid extraction kit (Shenggong Bioengineering Co., LTD., Shanghai, China) was used

143   to extract total DNA from fresh samples (The extraction method is shown in the supplementary material).

144   The abundance of HRGs in the surface soil of SMFC and OMFC anode after operation was analyzed

145   using an SYBR Green real-time fluorescence quantitative PCR system (7500, Thermo Fisher, USA)

146   (Wang et al., 2023c). The soil of OMFC was used for comparison. The detected genes included HRGs

147   *(chrA, chrB, chrR, recG, nfsA, zupT, fpvA)* and MGEs (*intI, tnpA02, tnpA04, tnpA05*). The primer

148   sequences are provided in Table S2. The specific detection steps were as follows: pre-denaturation at 95°

149   C for 30 s, denaturation at 95°C for 5 s, and annealing and extension at 60°C for 30 s. Forty cycles were

150   performed to make three replicates, and 16S rRNA was used as the internal reference gene. The relative

151   gene expression results were analyzed using the $2^{\wedge}(-\Delta\Delta Ct)$ method, which is commonly used for relative

152   quantification, where $\Delta\Delta Ct$ = (Ct target gene - Ct internal reference gene) experimental group - (Ct target

153   gene - Ct internal reference gene) control group.

2.6 Data analysis

The experimental data were evaluated using one-way analysis of variance (ANOVA) based on three tests. The mean values and standard deviations were calculated using SPSS 22.0 software (IBM, USA). A significance level of $P<0.05$ was considered statistically significant, while $P<0.01$ was defined as highly statistically significant. Graphs were plotted using Origin 2022 software.

3.   Results

3.1 Electrodes characterization

As demonstrated in Fig. S2, Fig. 1, and Fig. 2, the raw GF had smooth surfaces with C, and O as the main elements (Fig. S2). After Fe_3O_4 loading, black patches constituted with spherical particles appeared, bringing Fe (13.17%) and O (19.97%) on the GF surface (Fig. 1a-c and Table S3). XPS revealed that peaks of the cathode GF loaded with catalyst at 710.80 and 724.40 eV were consistent with typical Fe_3O_4 peaks (Fig. 2a-b), indicating its successful loading. The CV curves of the cathode (Fig. 2c) presented an obvious oxidation peak at 0.85 V, indicating its excellent electrochemical performance.

Chromium exists mainly in the III and VI oxidation states in soil. The peaks at 576.90 eV and 579.00 eV are typical peaks of Cr(III) and Cr(VI), respectively. After operation, the typical peaks of Cr(III) and Cr(VI) can be observed on the X-ray energy spectra of both cathode and anode, and Cr(VI) and Cr(III) are present on the cathode and cathode of SMFC (Fig. 2d-e). The results showed that at least the valence state of Cr changed on the electrode and Cr(VI) was reduced and fixed by the electrode (Kim et al., 2017). GF was found loaded with many soil elements including Cr, Na, Mg, and Ca (Table S3). SEM also observed many microorganism cells and extracellular organic-like substances, implying the biofilm formation on the cathode (Fig. 1d-f).

175   As presented in Fig. S2C, the raw aluminum foam showed a rough porous structure with mainly Al

176   and O on the surface (Table S3). After loading EAB, many spherical and rod-shaped bacteria were

177   observed, indicating that aluminum foam has a good capacity to carry microorganisms (Fig. 1g-i). After

178   the operation, many millimeter-scale soil particles were embedded in the anode interspace, indicating the

179   intense mass transfer between the anode and soil (Fig. 1j-l).

180
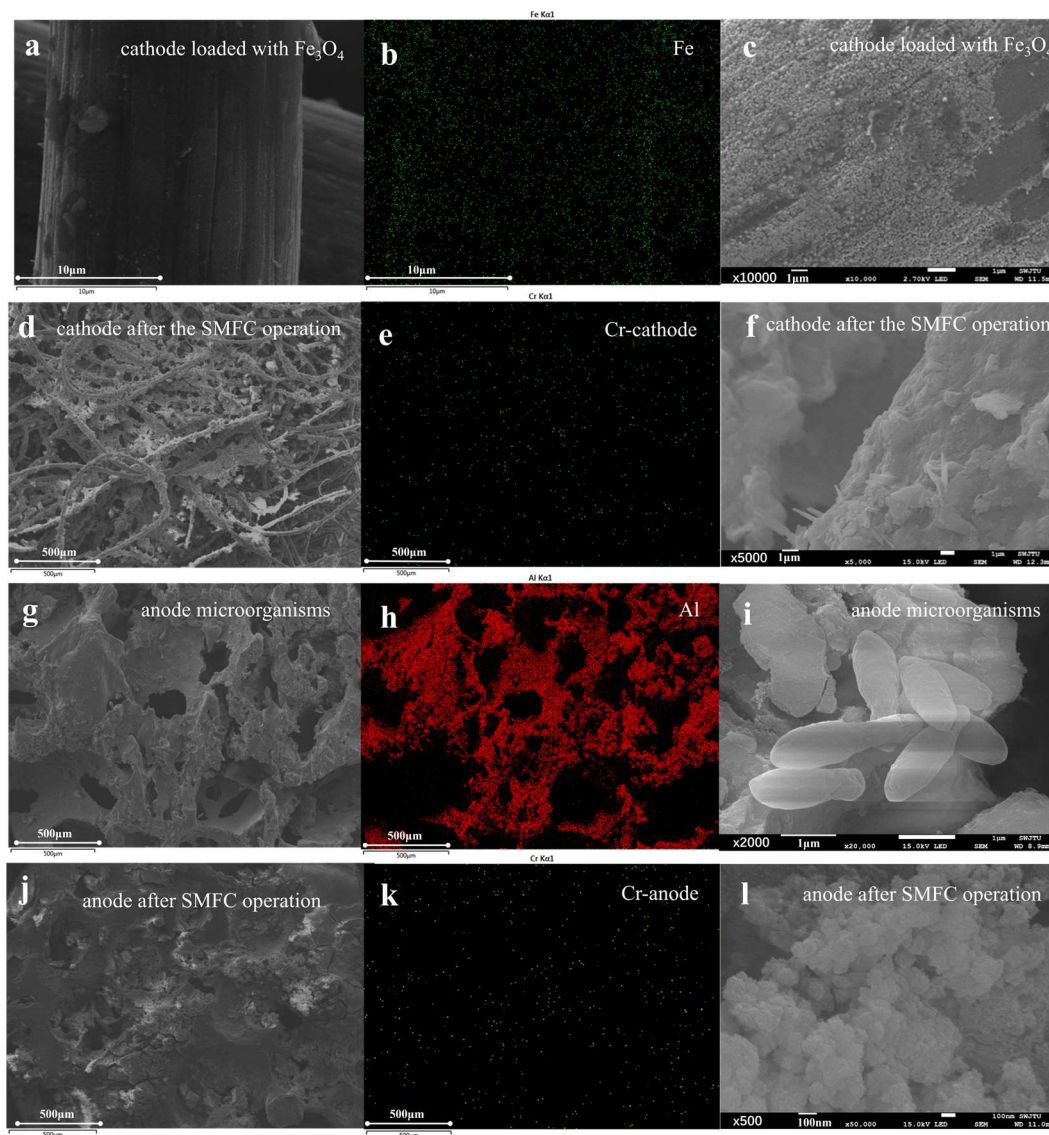
181   **Fig. 1** Characterization of electrode materials before and after operation by SEM and EDS. (a-c) SEM

182   and EDS images of cathode loaded with Fe_3O_4; (d-f) SEM and EDS images of cathode after the SMFC

183   operation; (g-i) SEM and EDS images of anode microorganisms; (j-l) SEM and EDS images of the anode

184   after SMFC operation. (Note: The first column is the SEM image, the second column is the corresponding

185   EDS, and the third column is the corresponding enlarged SEM image.)

186
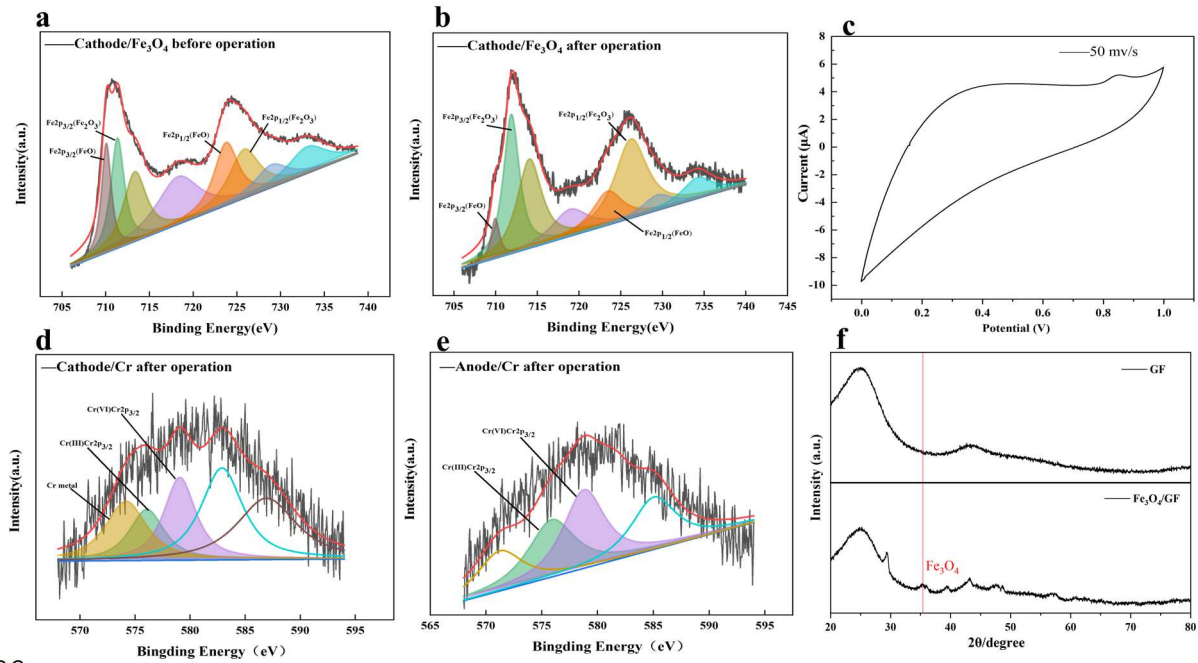
187   **Fig. 2** Characterization of electrode materials. (a-b) Fe2p spectra of cathode/Fe$_3$O$_4$ composite cathode,

188   (c) cyclic voltammetry (CV) curve of cathode/Fe$_3$O$_4$, (d-e) Cr2p spectra of GF composite cathode and

189   Anodic Aluminum foam after operation, (f) XRD spectrum of the cathode-Fe$_3$O$_4$.

190
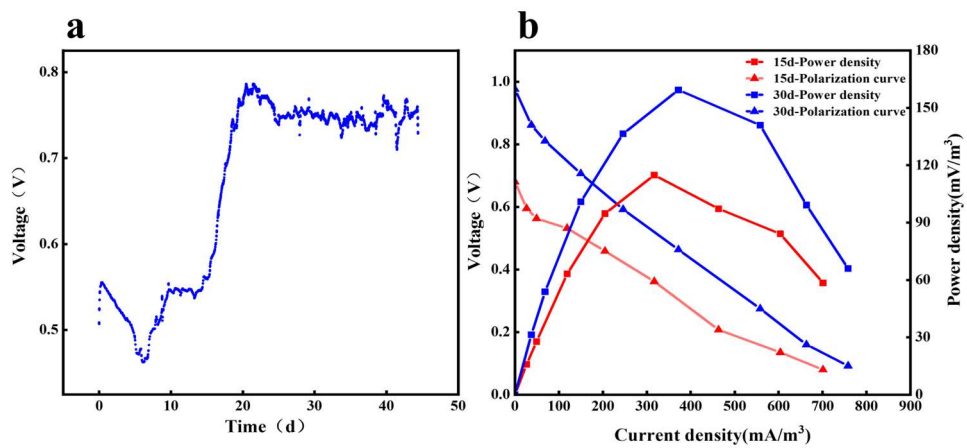
191   **Fig. 3** Power generation performance of SMFC. (a) SMFC output voltage distribution, (b) 15-day vs. 30-

192   day polarization curves and power density curves of the SMFC.

3.2 Electricity Generation Performance

Initially, CMFC showed a working circuit voltage (WCV) of 0.55 V and an open circuit voltage (OCV) of 0.68 V (Fig. 3a). In the first week, WCV dropped quickly to 0.45 V but bounced back and stabilized at 0.75 V on day 25, implying the adaption process of the anode microbes in the soil. We reasonably concluded that in the complex heterogeneous environment of soil, the anodic EAB needs some time to adapt to fluctuating environmental conditions facing environmental disturbances. During SMFC operation, the anode microbial community could be gradually selected and enriched, and a stable adaptive community is formed, so the SMFC voltage tends to be stable. This conjecture is also reflected in subsequent results.

On day 15 (OCV of 0.67 V) and day 30 (OCV of 0.97 V), a series of resistors (50~10 000 Ω) was connected to the electrodes to determine the polarization curves and power density of the SMFC. As shown in Fig. 3b, the power density increased and decreased with the elevation of external resistance. At 510 Ω, the power density reached a maximum of 114.90 mW/m^3 (73.50 mW/m^2) on day 15 and 159.40 mW/m^3 (102.00 mW/m^2) on day 30 (Table S4). The result indicated that the electrochemical performance of SMFC enhanced gradually probably due to the microbial adaption. Even after 45 days, the CMFC still had a WCV of around 0.75 V, indicating its substantial and stable electricity-producing capacity. Compared with the literature, the SMFC in the current work has an outstanding power generation capacity (Table S5).

3.3 Cr(VI) reduction and immobilization during operation

The forms and speciations of HMs determine their bioavailability and toxicity (Jia et al., 2022). After operation, Cr forms in soils were significantly changed ($P<0.05$) (Fig. 4). In CMFC, the acid-soluble Cr

214 decreased substantially by 97.44%, the oxidizable and reducible fractions did not change significantly,

215 while the residual form of Cr increased by 88.89% (Fig. 4a). However, in NMFC, the acid-soluble Cr

216 increased substantially by 61.54% on day 35. In OMFC, the acid-soluble Cr increased before decreasing,

217 which was opposite to its oxidizable state. On day 35, the Cr bioavailability of OMFC (11.90%) and

218 NMFC (18.90%) was 3866-6200 folds of CMFC (0.30%). It is inferred that the electric field and the

219 microbial communities' evolvement may lead to better Cr immobilization and transform Cr into less toxic

220 forms.

221 In the meantime, the Cr(VI) concentration (Fig. 4c) dropped in all the groups, and Cr (VI) in CMFC

222 soil was significantly lower than OMFC and NMFC ($P<0.05$) after the experiment. On day 35, CMFC

223 showed 13.59% and 20.87% higher Cr(VI) elimination than OMFC and NMFC, respectively. The

224 overlying water was initially free of Cr. During the experiment (Fig. S3), 0.21~12.72 mg/L Cr was

225 determined, which could be released from the soil. A low level of Cr(VI) (less than 3.15 mg/L) was

226 detected but vanished later (day 15), which could be attributed to the dynamic adsorption-desorption of

227 soil particles and electrodes.

228
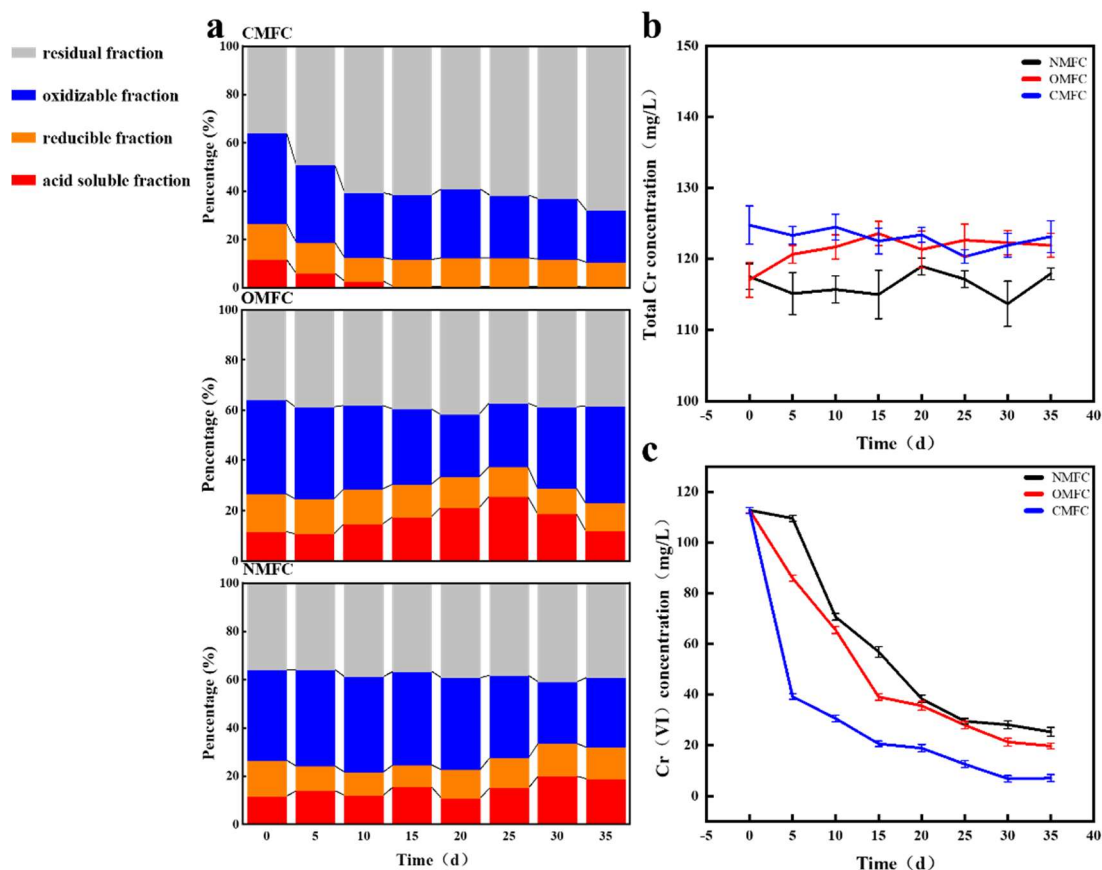
229   **Fig. 4** Cr speciation and transformation during SMFC operation. (a) Percentage share of Cr in different

230   chemical fractions in CMFC, OMFC, and NMFC soil; Changes in soil (b) total chromium and (c) Cr(VI)

231   concentrations during SMFC operation.

232   **3.4 Soil properties**

233   3.4.1 Soil Physicochemical Property

234   The soil pH decreased in all the groups (Fig. S4A). The soil pH of CMFC decreased fastest from the

235   initial 7.71 to about 6.83 on day 35, with a minimum of 6.77 on day 30, which was 0.14-7.87% lower

236   than others ($P<0.05$). During the experiment, oxygen in the flooded soil decreased rapidly due to

237   microbial consumption, and acidic products (e.g., low-molecule organic acids) were produced to increase

238   soil acidity. Microorganisms (especially EABs) decompose soil organic matter and release a large

239   number of electrons and protons, making oxidizing substances such as nitrate and high valence metals

240   (Fe(III), Mn(IV), and Cr(VI)) to accept electrons for reduction, causing protons (H$^+$) accumulation (He

241   et al., 2016). Such a phenomenon was more intense in CMFC due to the rapid electron transfer through

242   wire to the cathode, leaving protons elevated near the anode.

243   In all the groups, EC increased rapidly from the initial 1.55 ms/cm before stabilizing (Fig. S4B),

244   which maximized 2.60, 2.40, and 2.40 ms/cm in CMFC, OMFC, and NMFC (P>0.05), respectively. The

245   rapid increase in EC could be attributed to the inundation that increased the soluble salt content of the

246   soils. The electromigration in the MFC electric field may also increase soil mass transfer and positively

247   affect soil electrical conductivity (Zhang et al., 2020).

248   3.4.2 Soil Biochemical Response

249   Soil enzyme activity is an important index to evaluate soil environmental change. Soil enzymes, as

250   biocatalysts involved in biochemical reactions, play an important role in nutrient mineralization,

251   decomposition of organic matter, and nutrient cycling (Chen et al., 2024; Liu et al., 2018). The DHA

252   activity increased significantly in all three groups (2 244.00~3 138.00% higher than the initial value) and

253   continuously (P<0.05) (Fig. S5A). Under flooding, microbial activity changed from aerobic to anaerobic,

254   leading to a sharp decline in soil redox potential, accompanied by the stimulation of soil DHA (Sardans

255   and Peñuelas, 2005). During operation, urease activity in CMFC showed a gradual increase (2.70~12.40%

256   higher than day 0 from days 10~35), while it in OMFC and NMFC showed a slight decrease (6.10~7.10%

257   lower than day 0 from days 5~35) (Fig. S5B). SMFC electric field and Fe(II) promote extracellular

258   electron transfer (EET) (Chen et al., 2023a), which promotes the enrichment of ammonia-nitrogen

259   transforming bacteria in soil could have caused the higher urease activity in CMFC than NMFC and

260   OMFC (P<0.05). Soil invertase activity decreased initially but increased later for CMFC and OMFC, but

showed an opposite trend for NMFC. After operation, CMFC had a significantly higher invertase activity

than others ($P<0.05$) (Fig. S5C). Soil ACP showed a similar trend with urease, with CMFC continuously

increasing by 13.20~48.90% and considerably higher than OMFC and NMFC (Fig. S5D). The dynamic

measurement of soil enzyme activity in SMFC helps us to understand and analyze the changing state of

soil microecology.

3.5 SMFC operation reshaped soil microbial community

Microbial community structures in the electrodes were analyzed, which obtained 15 dominant phyla and

50 dominant genera (>1.0%). Overall, *Firmicutes* (73.93%), *Proteobacteria* (62.53%), and *Chloroflexi*

(21.73%) were found the dominant phyla, while *Bacteroides* (21.48%), *Enterococcus* (17.26%), and

Hyphomicrobium (15.34%) were the dominant genera.

The alpha diversity analysis indicated a significant difference in the microbial community among the

samples (Fig. 5). The higher chao1 index in soils than the electrodes demonstrated higher microbial

richness. Most of the alpha index in OMFC-A and OMFC-C were significantly higher than CMFC-A and

CMFC-C, demonstrating a higher microbial richness and diversity in OMFC. The results indicated the

different microbial evolution patterns in different electrodes and the selection effect of the electricity

field during CMFC operation. The Venn diagram (Fig. S6) found no OTU coincidence among the

samples, indicating their obvious specificity. In comparison, 2130 OTUs were shared by CMFC-S,

OMFC-S, and NMFC-S, indicating the similarity of the soil microbial community (Fig. S6B). 45 OTUs

were shared by Raw-A, CMFC-A, and OMFC-A, accounting for 45.92%, 1.95%, and 1.16%,

respectively, indicating the successful colonization and development of the preloaded EABs.

-A present anode   **-S present soil**
-C present cathode   **-Raw-A present anode before operation**
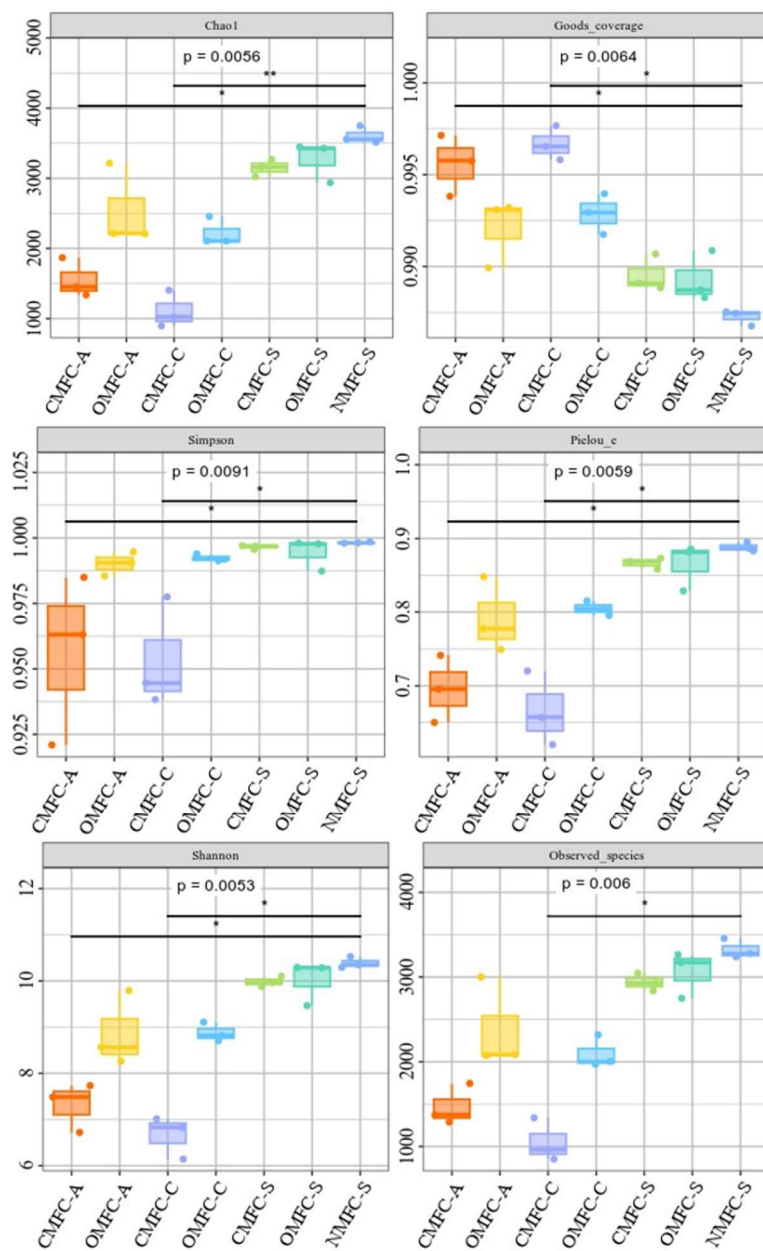
     Fig. 5 Alpha diversity analysis of the electrodes and soils

283
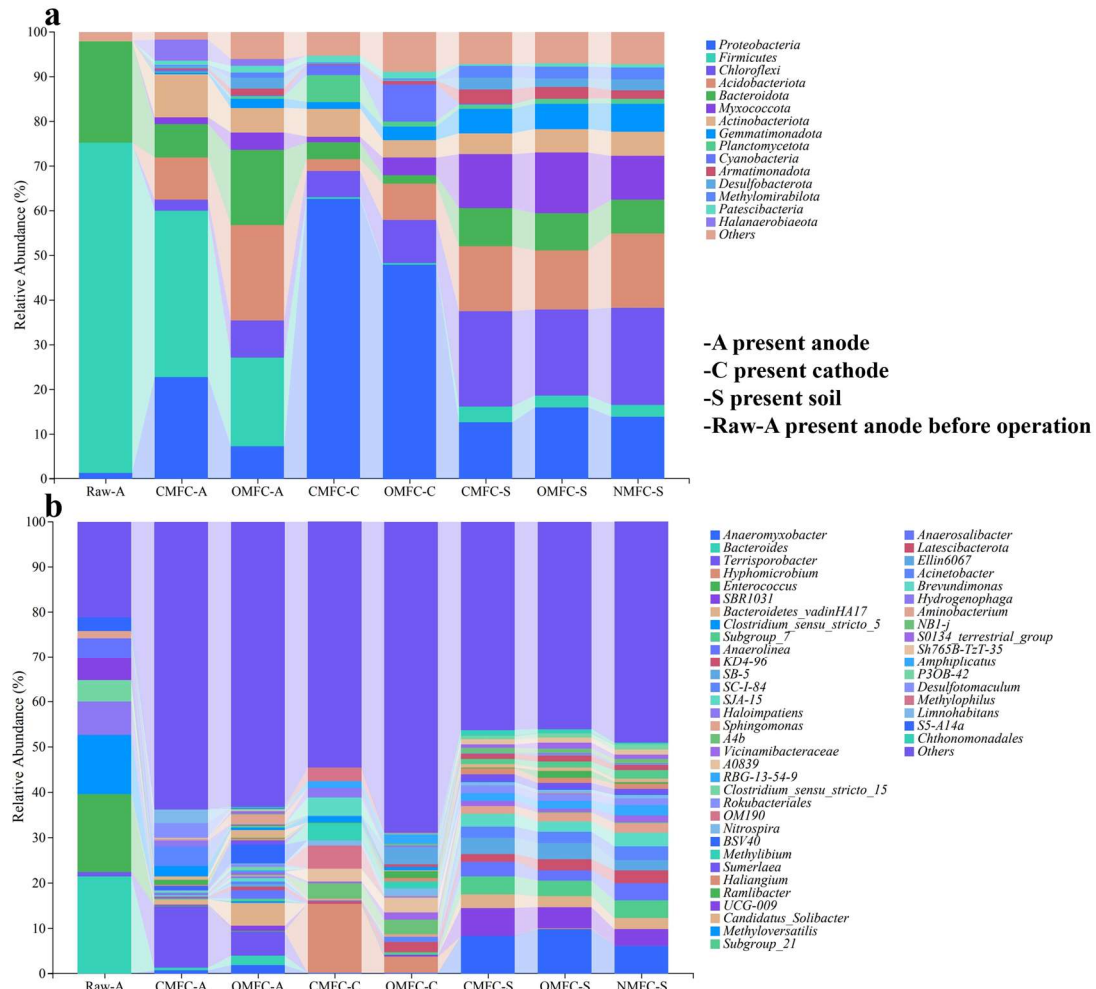
284   **Fig. 6** Microbial community structure is based on (a) the phylum level and (b) the genus level.

285   3.5.1 Soil microbial community reshaping on phylum level

286   At the phylum level (Fig. 6a), before the operation, the anode was dominated by *Firmicutes* (73.93%),

287   *Bacteriodota* (22.74%), and *Proteobacteria* (1.27%). After the operation, *Firmicutes* and *Bacteriodota*

288   decreased by 49.83% and 66.84% in CMFC-A, and 73.20% and 26.52% in OMFC-A, respectively. While

289   *Proteobacteria* increased by 1 698.43% in CMFC-A and 475.59% in OMFC-A. Besides, many other

290   phyla emerged, including *Acidobacteriota* (9.41%~21.40%), *Actinobacteriota* (0.23%~9.52%),

291   *Halanaerobiaeota* (1.48%~4.77%), *Myxococcota* (1.51%~3.93%), *Chloroflexi* (0.01%~2.57%),

292   indicating the increased microbial diversity, probably due to the penetration of soil indigenous microbe.

The cathode was free of microorganisms initially. However, many phyla were observed after the operation. The CMFC-C was dominated by *Proteobacteria* (62.53%), *Actinobacteriota* (6.24%), *Planctomycetota* (6.04%), *Chloroflexi* (5.88%), and *Bacteroidota* (3.81%), while OMFC-C was dominated by *Proteobacteria* (47.93%), *Chloroflexi* (9.75%), *Cyanobacteria* (8.30%), *Acidobacteriota* (8.01%), *Actinobacteriota* (3.97%), *Myxococcota* (3.92%), and *Gemmatimonadota* (2.87%). The *Proteobacteria* phylum was rich in EABs, its advantage in both electrodes of CMFC indicated that SMFC operation was favorable for EAB colonization and development. All the soils were dominated by *Chlorobacteria*, *Acidobacteria*, *Proteobacteria*, *Bacteroidetes*, and *Myxococcota*, and the difference was not significant.

3.5.2 Soil microbial community reshaping on genus level

At the genus level (Fig. 6b), MFC operation presented a selection effect, with *Terrisporobacter* increasing from 0.81% to 13.71% and *Bacteroides* decreasing from 12.48% to 0.53% in CMFC anode. Compared with the Raw-A, many EABs in CMFC-A decreased, including *Clostridium_sensu_ stricto_5* (from 12.99% to 0.05%), *Clostridium_sensu_stricto_15* (from 4.70% to 0.47%), *Enterococcus* (from 17.26% to 0.03%) (Choi, 2022; Zhang et al., 2023).

However, the *Desulfotomaculum* in CMFC-A increased to 3.32% compared with 0.003% in the soil (CMFC-S). Besides, soil indigenous bacteria including *Ramlibacter, Methyloversatilis,* and *Acinetobacter* colonized in the anode and elevated by 4.89~1 579.00 fold compared with soil. Nevertheless, multiple dominant genera in the soils decreased in CMFC-A than in OMFC-A. For example, *SBR1031*, *Bacteroidetes_vadinHA17*, and *Anaerolinea* were significantly increased in soil, but less in CMFC-A and OMFC-A. The electric field action to a certain extent helped the anode to resist

314   external microbial intrusion to ensure the stability of the anodic microbial community.

315   During operation, the prolonged interaction between the soil and water phases resulted in the

316   gradually evolving unique biofilm structure of the cathode. For instance, *Hyphomicrobium* (3.56~15.34%

317   in soils), an aerobic chemoheterotroph capable of degrading a wide range of organics, accounted for

318   15.34% and 3.56% of CMFC-C and OMFC-C, respectively (He et al., 2019). *Hydrogenophaga*, a gram-

319   negative bacteria capable of denitrification and Cr(VI) reduction, accounted for 2.07% of CMFC-C

320   (Wang et al., 2022). Meanwhile, the SMFC operation caused the enrichment of several resistant bacteria.

321   *Subgroup_7*, a typical HM-tolerant bacterium (Li et al., 2023a), was enriched in both cathode and soil.

322   *Acinetobacter* and *Limnohabitans*, also tolerators that carry HRGs and ARGs, were found 4.31% and

323   3.03% in CMFC-A (Dahal et al., 2023; Zhang et al., 2021).

324   The increase of iron in soil and water due to the use of Fe_3O_4 as cathode catalyst may be responsible

325   for the enrichment of *Terrisporobacter* and *Anaeromyxobacter* in the CMFC-A and OMFC-A. They were

326   found closely associated with Fe^{3+} reduction to gain energy in various environments (Lin et al., 2007;

327   Wang et al., 2020b).

328   3.5.3 Soil metal resistance gene variation

329   Under Cr(VI) stress, certain microbes would utilize pathways like specific or non-specific Cr(VI)

330   reduction, free radical detoxification, DNA damage repair, etc. to survive in toxic environments (Morais

331   et al., 2011). Using qPCR analysis, the abundance of typical HRGs and MGEs in the anodic soils was

332   determined (Fig. 7a), among which *chrA, chrB, and chrR*, are typical HRGs involved in Cr response,

333   while *IntI, tnpA02, and tnpA05* are common mobile genetic elements (MGEs) that varied greatly during

334   operation ($P<0.05$). Compared with OMFC and NMFC, *chrA* in CMFC increased by 237.83% and

335   3414.34%, *chrB* by 141.52% and 153.63%, *chrR* by 221.86% and 839.41%, *IntI* by 151.77% and

336   167.91%, *tnpA02* by 331.86% and 1118.97%, and *tnpA05* by 416.91% and 99.54%. Changes in soil

337   resistance characteristics during SMFC operation may be directly or indirectly caused by environmental

338   factors and resistant microbial communities.

339   The elevation of HRGs and MGEs could be due to the enrichment of multiple metal-resistant bacteria

340   (MRB) such as *Acinetobacter, Limnohabitans,* and *Brevundimonas*. Moreover, the anodic

341   *Desulfotomaculum*, which accounted for 3.23% of CMFC-A, is a typical sulfate-reducing bacterium

342   (SRB) that produces H_2S, a natural signaling molecule that contributes to tolerance triggering,

343   maintenance, and diffusion through community sensing, which facilitates HRG elevation through HGT

344   (Shatalin et al., 2021). Besides, Cr(VI) reducing bacteria like *Hydrogenophaga* (1.31% in CMFC-A) may

345   also up-regulate the Cr reductase gene *chrR* (Sundarraj et al., 2023).

346   Furthermore, pH changes may also affect soil resistance characteristics. Liu et al. (2023c) observed

347   the abundance of multidrug efflux pump genes in the acid soil was significantly positively correlated

348   with soil acidity. The intensified proton generation and accumulation in CMFC could have led to the

349   HRG elevation. In addition, HMs toxicity exerts direct selective pressure, which affects microbial

350   community structure and their function, leading to the thriving of tolerators like *Desulfotomaculum sp,*

351   *Hydrogenophaga*, and *Methylophilus* (Hernández-Ramírez et al., 2018), hence the spontaneous HRG

352   elevation (Wang et al., 2023c).
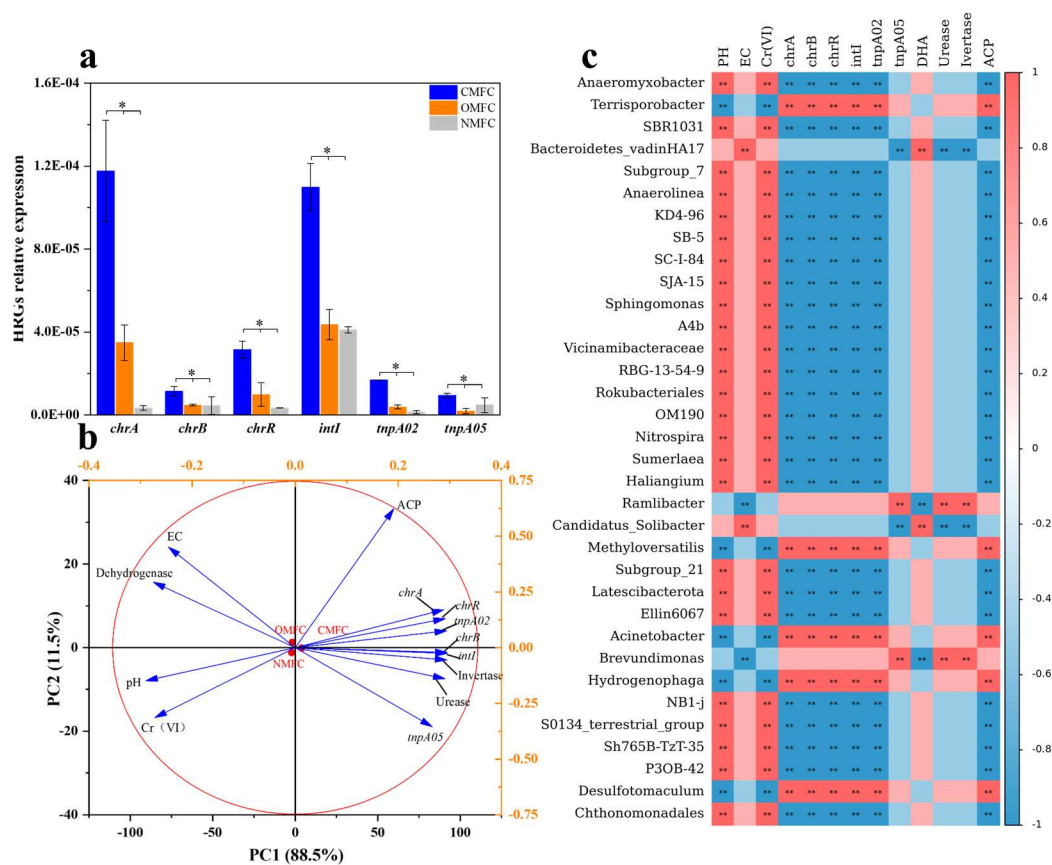
Fig. 7 HRG variation and correlation analysis of dominant bacteria, HRG, and soil enzymatic activity.

(a)qPCR results of HRG changes in soil around anode-soil after SMFC operation (*chrA*, *chrB*, *chrR*, *intI*, *tnpA02*, *tnpA05*). Different letters denote significant differences among treatments (*P*<0.05); (b) principal component analysis (PCA) of SMFC soil physicochemical properties with Enzyme activity, HRGs, and native bacterial genera and (c) Spearman's correlation heatmap (mean relative abundance>1%). * *P*<0.05, according to LSD test (mean±S.E., n=3); ** *P*<0.01.

3.6 Correlation analysis

To visually analyze the correlation between bacterial communities and environmental factors, spearman correlation analysis and principal component analysis (PCA) were conducted (Fig. 7). Spearman correlation analysis (Fig. 7c) isolated four main bacterial genera clusters, which further revealed the correlation of environmental factors (pH, EC), soil enzyme activities (DHA, Urease, Invertase, ACP),

365 Cr(VI), and HRGs (*chrA, chrB, intI, tnpA02, tnpA05*) with the microbial community.

366 Cluster 1 (*Terrisporobacter, Methyloversatilis, Acinetobacter, Hydrogenophaga, and Desulfotomaculum*)

367 was positively correlated with HRGs (*chrA, chrB, intI, tnpA02*) and ACP ($P<0.01$), but negatively

368 correlated with pH and Cr(VI) ($P<0.01$), suggesting they may contribute to HGT and HRGs enrichment.

369 Cluster 2 (*Anaeromyxobacter, Subgroup_7, Anaerolinea, SB-5, Sphingomonas,* etc.) was negatively

370 correlated ($P<0.01$) with HRGs (*chrA, chrB, intI, tnpA02*) and ACP, but positively correlated with pH

371 and Cr(VI) ($P<0.01$). Cluster 3 (*Bacteroidetes_vadinHA17* and *Candidatus_Solibacter*) was positively

372 correlated ($P<0.01$) with soil EC and DHA. Cluster 4 (*Ramlibacter*, and *Brevundimonas*) were positively

373 correlated with urease and invertase but negatively correlated with EC.

374 PCA analysis (Fig. 7b) also indicated a close correlation between environmental factors, in which soil

375 pH, EC, Cr(VI) concentration, and DHA were positively correlated with each other but negatively

376 correlated with urease, ACP, invertase, and HRGs. Especially, Cr(VI) was significantly negatively

377 correlated with HRGs ($P<0.01$), which could be partially explained by the tolerators thriving and Cr(VI)

378 reduction during SMFC operation.

379 **4.   Discussion**

380 In this study, Cr(VI) reduction, microbial community variation, and HRG fate in SMFC were investigated

381 for the first time. The results proved that SMFC was an effective method to eliminate Cr(VI) (93.76%),

382 immobilize Cr (97.44%), and generate electricity (0.97 V).

383 Microorganisms have developed efficient detoxification strategies to counteract the toxic effects of

384 heavy metal stress (Rouch et al., 1995; Tan et al., 2020). In the SMFC system, Cr(VI) reduction was a

385 synergic result of adsorption/biosorption (including the adsorption of anode and cathode materials,

surface catalyst adsorption, and microbial membrane adsorption), bioelectrochemistry reduction, and

microbial reduction (including intracellular sequestration, export, reduced permeability, extracellular

sequestration, and extracellular detoxification) (Fig. 8). The preloading of Fe_3O_4 and EABs on the

electrodes significantly improved Cr(VI) reduction and power generation by accelerating SMFC

stabilization. The detailed explanation is as follows:

The electricity-producing process of SMFC can inhibit HMs' release and migration in soil (Zhu et al.,

2019; Feng et al., 2024). In this study, Cr forms changed greatly from acid-soluble to a more stable

residual fraction with low toxicity. The Fe_3O_4-modified cathode not only directly adsorbs or reduces

Cr(VI) due to the high specific area and ferrous iron, but also enhances the electrochemical effect of the

system. The electrons derived from anodic microbial metabolism can directly reduce Cr(VI) in the soil

to Cr(III), while part of them is transmitted to the cathode, where Cr(VI) in the overlying water compete

with oxygen as electron acceptors and complete the current loop (Thapa et al., 2022).

In addition, microorganisms can also directly or indirectly reduce or fix Cr. Biosorption, sulfide,

and hydroxide precipitation are the main immobilization mechanisms of HMs by microorganisms (Ma

et al., 2024). For example, *Desulfotomaculum sp.*, a typical SRB, enriched to 3.23% in CMFC-A, may

produce sulfide ions by reducing alienated sulfate, thus forming highly insoluble metal sulfide to fix Cr

through microorganism-induced sulfide precipitation (MISP). *Hydrogenophaga*, which dominated in

both electrodes, was a known Cr-reducing bacteria. Some of iron-reducing bacteria present in this study

(e.g., *Anaeromyxobacter* and *Terrisporobacter*) may also contribute to Cr(VI) reduction by participating

in the Fe cycle through EET, while the ferrous iron reduces Cr(VI). Additionally, the CMFC in this work

contains many genera capable of transforming nitrogen. For example, *Hyphomicrobium* dominated in

CMFC-C (15.34%), a typical denitrifying bacterium, can effectively reduce nitrate and nitrite (Ernst et al., 2021). *Methylophilus* accounted for 2.93% of CMFC-A but was much lower in other groups, which is a methylotrophic microorganism (Yang et al., 2020). The bacteria mentioned above were found with high urease-producing ability, whose enrichment not only improves soil urease activity and nutrient cycling but also immobilizes Cr through microorganism-induced carbonate precipitation (MICP) (Qian et al., 2017).

In addition to the reduction of Cr during SMFC operation, under electrochemical selection and HMs stress, the microbial community gradually evolved with higher richness and diversity, along with the HRG enrichment and nutrient cycling variation. Firstly, some soil indigenous bacteria were much lower in CMFC-A than OMFC-A, indicating the electric field contributed to the anode stability by preventing external bacteria intrusion and is less vulnerable to environmental fluctuations. The microbial community change is significantly related to HRG enrichment. Many EABs and MRBs are significantly enriched. For example, *Desulfotomaculum*, an SRB with a dual role of electroproduction and HMs reduction (Jiang et al., 2020; Yin et al., 2021). Other examples also include cumulative-resistant bacteria like *Acinetobacter* and *Limnohabitans* which are only enriched in the CMFC-A (Dahal et al., 2023; Al-Jabri et al., 2018). Their enrichment directly causes vertical gene transfer and HRG elevation. The Cr forms, soil physicochemical properties, soil enzyme activities, and microecological structure mirrored each other, helping to understand Cr transformation patterns and target the key factors affecting metal resistance changes.

HMs existence in soil can induce HGT occurrence and cause ARG elevation, which has become a major concern (Chen et al., 2023b; Fu et al., 2023). Sub-lethal levels of metal ions can increase mutation

428 rates and enrich de novo mutants with significant resistance to multiple antibiotics (Li et al., 2019). This

429 study focused on the toxic alleviation of a single HM (Cr) in SMFC, during which tolerator accumulation

430 caused considerable HRG enrichment. SMFC is an eco-friendly and cost-effective technology for the in-

431 situ bioremediation of contaminated soil/sediment and powering environmental sensors in remote areas.

432 It has the potential to be used as a novel early warning system for soil environmental hazards.

433 Nevertheless, before the commercialization of large-scale applications in the field, significant efforts

434 should be made to reveal the HRG enrichment mechanism during SMFC operation and pay attention to

435 ARG change under HMs contamination or HMs-antibiotic co-contamination.

436
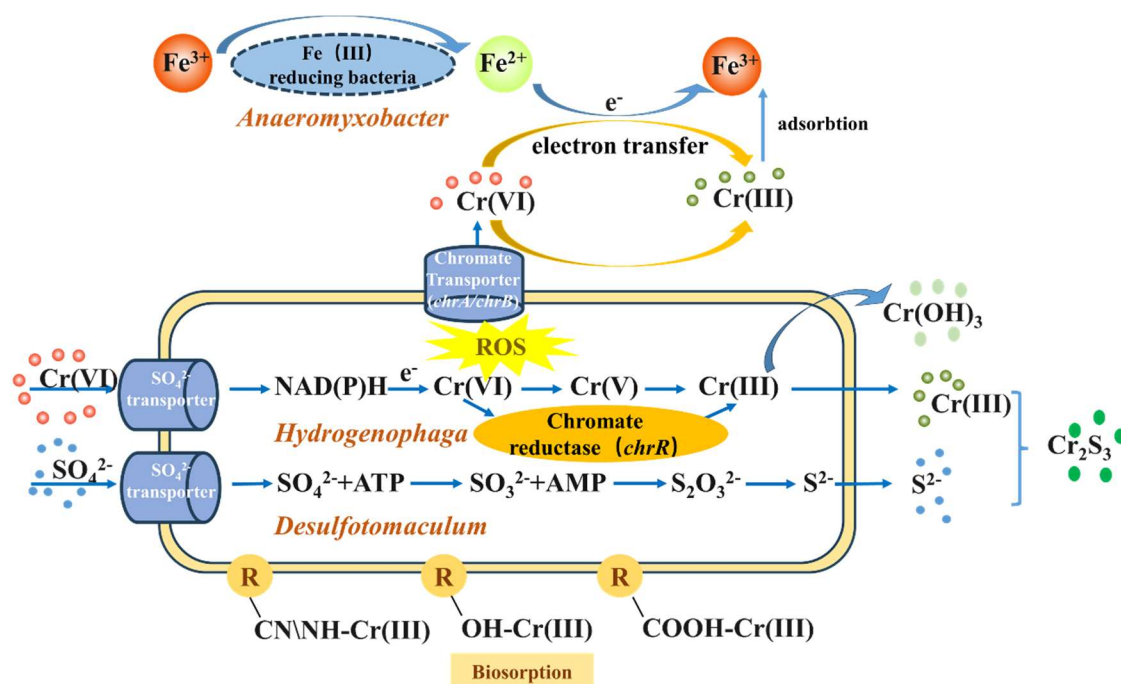
437 **Fig. 8** Cr(VI)reduction Mechanism during SMFC operation

5. Conclusion

439 During SMFC operation, the close interaction among the soil physicochemical properties, enzyme

440 activities, resistance genes, and microbial community structure determined the performance. The pre-

441 loading of Fe_3O_4 in the cathode and EAB in the anode greatly contributed to power production and Cr(VI)

442   elimination. Anodic microbial metabolism, cathodic redox, and the MFC electric field reduced or

443   immobilized Cr(VI) to eliminate its risk. The enrichment of multiple MRBs, such as *Acinetobacter,*

444   *Limnohabitans,* and *Desulfotomaculum*, resulted in HRG elevation, which contributes to microbial

445   adaptation and function but brings concerns for future application. This study provides a reference for

446   the remediation of HM-contaminated soil using MFC, which is conducive to promoting the practical

447   application of bioelectrochemical technology in the field.

448   **Author contribution:**

449   HN: Conceptualization, Investigation, and Writing; XL: Investigation, Visualization; PL: Investigation,

450   Visualization; HQ: Methodology; LJ: Writing-review and editing; SM: Writing-review and editing; MW:

451   Writing-review; FX: Funding acquisition, Supervision; HX: Funding acquisition, Supervision; CW:

452   Funding acquisition, Supervision.

453   **Acknowledgments**

454   This work was financially supported by the Sichuan Science and Technology Program (2024NSFSC0384

455   and 25NSFSC2362), the Government Guides Local Science and Technology Development Project of the

456   Tibetan Autonomous Region of China (XZ202401YD0001), the China Postdoctoral Science Foundation

457   (2022M712630), and the National Natural Science Foundation of China (No. 42207021). We thank Dr.

458   Weizhen Fang from the Analysis & Testing Center and Dr. Cuijuan Wang from the School of Chemistry,

459   Southwest Jiaotong University, for the technical support. We thank Lijuan Zhang from SCI-Go (www.sci-

460   go.com) for the XPS analysis.

Declaration of interests

The authors declare that they have no known competing financial interests or personal relationships

that could have appeared to influence the work reported in this paper.

Reference

AL-Jabri, Z., Zamudio, R., Horvath-Papp, E., Ralph, J. D., AL-Muharrami, Z., Rajakumar, K., and Oggioni, M. R.: Integrase-Controlled Excision of Metal-Resistance Genomic Islands in *Acinetobacter baumannii*, Genes, 9, 366, https://doi.org/10.3390/genes9070366, 2018.

Ashbolt Nicholas, J., Amézquita, A., Backhaus, T., Borriello, P., Brandt Kristian, K., Collignon, P., Coors, A., Finley, R., Gaze William, H., Heberer, T., Lawrence John, R., Larsson, D. G. J., McEwen Scott, A., Ryan James, J., Schönfeld, J., Silley, P., Snape Jason, R., Van den Eede, C., and Topp, E.: Human Health Risk Assessment (HHRA) for Environmental Development and Transfer of Antibiotic Resistance, Environ. Health Perspect., 121, 993-1001, https://doi.org/10.1289/ehp.1206316, 2013.

Bokulich, N. A., Kaehler, B. D., Rideout, J. R., Dillon, M., Bolyen, E., Knight, R., Huttley, G. A., and Gregory Caporaso, J.: Optimizing taxonomic classification of marker-gene amplicon sequences with QIIME 2's q2-feature-classifier plugin, Microbiome, 6, 90, https://doi.org/10.1186/s40168-018-0470-z, 2018.

Chen, C., Fang, Y., and Zhou, D.: Selective pressure of PFOA on microbial community: Enrichment of denitrifiers harboring ARGs and the transfer of ferric-electrons, Water Res., 233, 119813, https://doi.org/10.1016/j.watres.2023.119813, 2023a.

Chen, M., Cai, Y., Li, G., Zhao, H., and An, T.: The stress response mechanisms of biofilm formation under sub-lethal photocatalysis, Appl. Catal., B, 307, 121200, https://doi.org/10.1016/j.apcatb.2022.121200, 2022a.

Chen, P., Zhang, T., Chen, Y., Ma, H., Wang, Y., Liu, W., Wang, Y., Zhou, G., Qing, R., Zhao, Y., Xu, H., Hao, L., Wang, C., and Xu, F.: Integrated Chamber-free Microbial Fuel Cell for Wastewater Purification and Bioenergy Generation, Chem. Eng. J., 136091, https://doi.org/10.1016/j.cej.2022.136091, 2022b.

Chen, X., Du, Z., Song, X., Wang, L., Wei, Z., Jia, L., and Zhao, R.: Evaluating the occurrence frequency of horizontal gene transfer induced by different degrees of heavy metal stress, J. Cleaner Prod., 382, 135371, https://doi.org/10.1016/j.jclepro.2022.135371, 2023b.

Chen, Y., Zuo, M., Yang, D., He, Y., Wang, H., Liu, X., Zhao, M., Xu, L., Ji, J., Liu, Y., and Gao, T.: Synergistically Effect of Heavy Metal Resistant Bacteria and Plants on Remediation of Soil Heavy Metal Pollution, Water, Air, Soil Pollut., 235, 296, https://doi.org/10.1007/s11270-024-07100-w, 2024.

Choi, S.: Electrogenic Bacteria Promise New Opportunities for Powering, Sensing, and

Synthesizing, Small, 18, 2107902, https://doi.org/10.1002/smll.202107902, 2022.

Coetzee, J. J., Bansal, N., and Chirwa, E. M. N.: Chromium in Environment, Its Toxic Effect from Chromite-Mining and Ferrochrome Industries, and Its Possible Bioremediation, Exposure and Health, 12, 51-62, https://doi.org/10.1007/s12403-018-0284-z, 2020.

Cong, Y., Shen, L., Wang, B., Cao, J., Pan, Z., Wang, Z., Wang, K., Li, Q., and Li, X.: Efficient removal of Cr(VI) at alkaline pHs by sulfite/iodide/UV: Mechanism and modeling, Water Res., 222, 118919, https://doi.org/10.1016/j.watres.2022.118919, 2022.

Dahal, U., Paul, K., and Gupta, S.: The multifaceted genusAcinetobacter: from infection to bioremediation, J. Appl. Microbiol., 134, https://doi.org/10.1093/jambio/lxad145, 2023.

Deng, Y., Jiang, Y.-H., Yang, Y., He, Z., Luo, F., and Zhou, J.: Molecular ecological network analyses, BMC Bioinformatics, 13, 113, https://doi.org/10.1186/1471-2105-13-113, 2012.

Dimova, M., Iutynska, G., Yamborko, N., Dordevic, D., and Kushkevych, I.: Possible Processes and Mechanisms of Hexachlorobenzene Decomposition by the Selected Comamonas testosteroni Bacterial Strains, Processes, 10, 2170; https://doi.org/10.3390/pr10112170, 2022.

Ernst, C., Kayastha, K., Koch, T., Venceslau, S. S., Pereira, I. A. C., Demmer, U., Ermler, U., and Dahl, C.: Structural and spectroscopic characterization of a HdrA-like subunit from *Hyphomicrobium denitrificans*, The FEBS Journal, 288, 1664-1678, https://doi.org/10.1111/febs.15505, 2021.

Fan, C., Qian, J., Yang, Y., Sun, H., Song, J., and Fan, Y.: Green ceramsite production via calcination of chromium contaminated soil and the toxic Cr(VI) immobilization mechanisms, J. Cleaner Prod., 315, 128204, https://doi.org/10.1016/j.jclepro.2021.128204, 2021.

Fan, Q., Fan, L., Quach, W.-M., Zhang, R., Duan, J., and Sand, W.: Application of microbial mineralization technology for marine concrete crack repair: A review, J. Building Engineering, 69, 106299, https://doi.org/10.1016/j.jobe.2023.106299, 2023.

Farkas, D., Proctor, K., Kim, B., Avignone Rossa, C., Kasprzyk-Hordern, B., and Di Lorenzo, M.: Assessing the impact of soil microbial fuel cells on atrazine removal in soil, J. Hazard. Mater., 478, 135473, https://doi.org/10.1016/j.jhazmat.2024.135473, 2024.

Faust, K. and Raes, J.: Microbial interactions: from networks to models, Nat. Rev. Microbiol., 10, 538-550, https://doi.org/10.1038/nrmicro2832, 2012.

Feng, H., Jin, A., Yin, X., Hong, Z., Ding, Y., Zhao, N., Chen, Y., and Zhang, Y.: Enhancing biocathode denitrification performance with nano-Fe_3O_4 under polarity period reversal, Environ. Res., 241, 117641, https://doi.org/10.1016/j.envres.2023.117641, 2024.

Fu, Y., Zhu, Y., Dong, H., Li, J., Zhang, W., Shao, Y., and Shao, Y.: Effects of heavy metals and antibiotics on antibiotic resistance genes and microbial communities in soil, Process Saf. Environ. Prot., 169, 418-427, https://doi.org/10.1016/j.psep.2022.11.020, 2023.

Guo, S., Xiao, C., Zhou, N., and Chi, R.: Speciation, toxicity, microbial remediation and phytoremediation of soil chromium contamination, Environ. Chem. Lett., 19, 1413-1431, https://doi.org/10.1007/s10311-020-01114-6, 2021.

Gupta, S., Patro, A., Mittal, Y., Dwivedi, S., Saket, P., Panja, R., Saeed, T., Martínez, F., and Yadav, A. K.: The race between classical microbial fuel cells, sediment-microbial fuel cells, plant-microbial fuel cells, and constructed wetlands-microbial fuel cells: Applications and technology readiness level, Sci. Total Environ., 879, 162757, https://doi.org/10.1016/j.scitotenv.2023.162757, 2023.

Gustave, W., Yuan, Z.-F., Li, X., Ren, Y.-X., Feng, W.-J., Shen, H., and Chen, Z.: Mitigation effects of the microbial fuel cells on heavy metal accumulation in rice (Oryza sativa L.), Environ. Pollut., 260, 113989, https://doi.org/10.1016/j.envpol.2020.113989, 2020.

Hamdan, H. Z. and Salam, D. A.: Sediment microbial fuel cells for bioremediation of pollutants and power generation: a review, Environ. Chem. Lett., 21, 2761-2787, https://doi.org/10.1007/s10311-023-01625-y, 2023.

He, Q., Gui, J., Liu, D., Li, X., Li, P., and Quan, S.: Research progress of soil property′s changes and its impacts on soil cadmium activity in flooded paddy field, J. Agro-Environ. Sci., 35, 2260-2268, https://doi.org/10.11654/jaes.2016-0892, 2016.

He, S., Guo, H., He, Z., Yang, C., Yu, T., Chai, Q., and Lu, L.: Interaction of Lolium perenne and *Hyphomicrobium sp.* GHH enhances the removal of 17α-ethinyestradiol (EE2) from soil, J. Soils Sed., 19, 1297-1305, https://doi.org/10.1007/s11368-018-2116-y, 2019.

Hernández-Ramírez, K. C., Reyes-Gallegos, R. I., Chávez-Jacobo, V. M., Díaz-Magaña, A., Meza-Carmen, V., and Ramírez-Díaz, M. I.: A plasmid-encoded mobile genetic element from *Pseudomonas aeruginosa* that confers heavy metal resistance and virulence, Plasmid, 98, 15-21, https://doi.org/10.1016/j.plasmid.2018.07.003, 2018.

Irankhah, S., Abdi Ali, A., Mallavarapu, M., Soudi, M. R., Subashchandrabose, S., Gharavi, S., and Ayati, B.: Ecological role of Acinetobacter calcoaceticus GSN3 in natural biofilm formation and its advantages in bioremediation, Biofouling, 35, 377-391, https://doi.org/10.1080/08927014.2019.1597061, 2019.

Jia, J., Bai, J., Xiao, R., Tian, S., Wang, D., Wang, W., Zhang, G., Cui, H., and Zhao, Q.: Fractionation, source, and ecological risk assessment of heavy metals in cropland soils across a 100-year reclamation chronosequence in an estuary, South China, Sci. Total Environ., 807, 151725, https://doi.org/10.1016/j.scitotenv.2021.151725, 2022.

Jiang, Y., Shang, Y., Gong, T., Hu, Z., Yang, K., and Shao, S.: High concentration of Mn^{2+} has multiple influences on aerobic granular sludge for aniline wastewater treatment, Chemosphere, 240, 124945, https://doi.org/10.1016/j.chemosphere.2019.124945, 2020.

Kim, C., Lee, C. R., Song, Y. E., Heo, J., Choi, S. M., Lim, D.-H., Cho, J., Park, C., Jang, M., and Kim, J. R.: Hexavalent chromium as a cathodic electron acceptor in a bipolar membrane microbial fuel cell with the simultaneous treatment of electroplating wastewater, Chem. Eng. J., 328, 703-707, https://doi.org/10.1016/j.cej.2017.07.077, 2017.

Li, C., Huang, H., Gu, X., Zhong, K., Yin, J., Mao, J., Chen, J., and Zhang, C.: Accumulation of heavy metals in rice and the microbial response in a contaminated paddy field, J. Soils Sed., https://doi.org/10.1007/s11368-023-03643-3, 2023a.

Li, X., Gu, A. Z., Zhang, Y., Xie, B., Li, D., and Chen, J.: Sub-lethal concentrations of heavy metals induce antibiotic resistance via mutagenesis, J. Hazard. Mater., 369, 9-16, https://doi.org/10.1016/j.jhazmat.2019.02.006, 2019.

Li, Y., Lin, J., Wu, Y., Jiang, S., Huo, C., Liu, T., Yang, Y., and Ma, Y.: Transformation of exogenous hexavalent chromium in soil: Factors and modelling, J. Hazard. Mater., 480, 135799, https://doi.org/10.1016/j.jhazmat.2024.135799, 2024.

Li, Y., Chen, Y., Chen, Y., Qing, R., Cao, X., Chen, P., Liu, W., Wang, Y., Zhou, G., Xu, H., Hao, L., Wang, C., Li, S., Zhu, Y., Haderlein, S., and Xu, F.: Fast deployable real-time bioelectric dissolved oxygen sensor based on a multi-source data fusion approach, Chem. Eng. J., 475, 146064, https://doi.org/10.1016/j.cej.2023.146064, 2023b.

Lin, B., Hyacinthe, C., Bonneville, S., Braster, M., Van Cappellen, P., and Röling, W. F. M.: Phylogenetic and physiological diversity of dissimilatory ferric iron reducers in sediments of the polluted Scheldt estuary, Northwest Europe, Environ. Microbiol., 9, 1956-1968, https://doi.org/10.1111/j.1462-2920.2007.01312.x, 2007.

Liu, H., Xu, F., Xie, Y., Wang, C., Zhang, A., Li, L., and Xu, H.: Effect of modified coconut shell biochar on availability of heavy metals and biochemical characteristics of soil in multiple heavy metals contaminated soil, Sci. Total Environ., 645, 702-709, https://doi.org/ j.scitotenv.2018.07.115, 2018.

Liu, S., Feng, Y., and Li, H.: Degradation mechanism of saliferous compounding heavy metals-organic wastewater by manganese and iron cycling in the microbial fuel cell, Chem. Eng. J., 473, 145389, https://doi.org/10.1016/j.cej.2023.145389, 2023a.

Liu, S., Pu, S., Deng, D., Huang, H., Yan, C., Ma, H., and Razavi, B. S.: Comparable effects of manure and its biochar on reducing soil Cr bioavailability and narrowing the rhizosphere extent of enzyme activities, Environ. Int., 134, 105277, https://doi.org/10.1016/j.envint.2019.105277, 2020.

Liu, X.-C., Zhang, K.-X., Song, J.-S., Zhou, G.-N., Li, W.-Q., Ding, R.-R., Wang, J.,

Zheng, X., Wang, G., and Mu, Y.: Tuning Fe_3O_4 for sustainable cathodic heterogeneous electro-Fenton catalysis by acetylated chitosan, Proc. Natl. Acad. Sci., 120, e2213480120, https://doi.org/10.1073/pnas.2213480120, 2023b.

Liu, Z., Zhao, Y., Zhang, B., Wang, J., Zhu, L., and Hu, B.: Deterministic Effect of pH on Shaping Soil Resistome Revealed by Metagenomic Analysis, Environ. Sci. Technol., 57, 985-996, https://doi.org/10.1021/acs.est.2c06684, 2023c.

Ma, S., Mao, S., Shi, J., Zou, J., Zhang, J., Liu, Y., Wang, X., Ma, Z., and Yu, C.: Exploring the synergistic interplay of sulfur metabolism and electron transfer in Cr(VI) and Cd(II) removal by *Clostridium thiosulfatireducens*: Genomic and mechanistic insights, Chemosphere, 352, 141289, https://doi.org/10.1016/j.chemosphere.2024.141289, 2024.

Mandal, S., Sarkar, B., Bolan, N., Ok, Y. S., and Naidu, R.: Enhancement of chromate reduction in soils by surface modified biochar, J. Environ. Manage., 186, 277-284, https://doi.org/10.1016/j.jenvman.2016.05.034, 2017.

Men, C., Liu, R., Xu, F., Wang, Q., Guo, L., and Shen, Z.: Pollution characteristics, risk assessment, and source apportionment of heavy metals in road dust in Beijing, China, Sci. Total Environ., 612, 138-147, https://doi.org/10.1016/j.scitotenv.2017.08.123, 2018.

Morais, P. V., Branco, R., and Francisco, R.: Chromium resistance strategies and toxicity: what makes *Ochrobactrum tritici 5bvl1* a strain highly resistant, BioMetals, 24, 401-410, https://doi.org/10.1007/s10534-011-9446-1, 2011.

Morales-Benítez, I., Montoro-Leal, P., García-Mesa, J. C., López Guerrero, M. M., and Vereda Alonso, E.: New magnetic chelating sorbent for chromium speciation by magnetic solid phase extraction on-line with inductively coupled plasma optical emission spectrometry, Talanta, 256, 124262, https://doi.org/10.1016/j.talanta.2023.124262, 2023.

Qian, X., Fang, C., Huang, M., and Achal, V.: Characterization of fungal-mediated carbonate precipitation in the biomineralization of chromate and lead from an aqueous solution and soil, J. Cleaner Prod., 164, 198-208, https://doi.org/10.1016/j.jclepro.2017.06.195, 2017.

Rani, L., Kaushal, J., and Lal Srivastav, A.: Biochar as sustainable adsorbents for chromium ion removal from aqueous environment: a review, Biomass Convers. Biorefin., https://doi.org/10.1007/s13399-022-02784-8, 2022.

Rouch, D. A., Lee, B. T. O., and Morby, A. P.: Understanding cellular responses to toxic agents: a model for mechanism-choice in bacterial metal resistance, J. Ind. Microbiol., 14, 132-141, https://doi.org/10.1007/BF01569895, 1995.

Sardans, J. and Peñuelas, J.: Drought decreases soil enzyme activity in a Mediterranean Quercus ilex L. forest, Soil Biol. Biochem., 37, 455-461, https://doi.org/10.1016/j.soilbio.2004.08.004, 2005.

Shatalin, K., Nuthanakanti, A., Kaushik, A., Shishov, D., Peselis, A., Shamovsky, I., Pani, B., Lechpammer, M., Vasilyev, N., Shatalina, E., Rebatchouk, D.,

Mironov, A., Fedichev, P., Serganov, A., and Nudler, E.: Inhibitors of bacterial H$_2$S biogenesis targeting antibiotic resistance and tolerance, Science, 372, 1169-1175, https://doi.org/10.1126/science.abd8377, 2021.

Sundarraj, S., Sudarmani, D. N. P., Samuel, P., and Sevarkodiyone, S. P.: Bioremediation of hexavalent chromium by transformation of *Escherichia coli DH5α* with chromate reductase (*ChrR*) genes of *Pseudomonas putida* isolated from tannery effluent, J. Appl. Microbiol., 134, lxac019, https://doi.org/10.1093/jambio/lxac019, 2023.

Tan, H., Wang, C., Zeng, G., Luo, Y., Li, H., and Xu, H.: Bioreduction and biosorption of Cr(VI) by a novel Bacillus sp. CRB-B1 strain, J. Hazard. Mater., 386, 121628, https://doi.org/10.1016/j.jhazmat.2019.121628, 2020.

Thapa, B. S., Kim, T., Pandit, S., Song, Y. E., Afsharian, Y. P., Rahimnejad, M., Kim, J. R., and Oh, S.-E.: Overview of electroactive microorganisms and electron transfer mechanisms in microbial electrochemistry, Bioresour. Technol., 347, 126579, https://doi.org/10.1016/j.biortech.2021.126579, 2022.

van Hoek, A. H., Mevius, D., Guerra, B., Mullany, P., Roberts, A. P., and Aarts, H. J.: Acquired Antibiotic Resistance Genes: An Overview, Front. Microbiol., 2, https://doi.org/10.3389/fmicb.2011.00203, 2011.

Wang, C., Zhou, Z., Liu, H., Li, J., Wang, Y., and Xu, H.: Application of acclimated sewage sludge as a bio-augmentation/bio-stimulation strategy for remediating chlorpyrifos contamination in soil with/without cadmium, Sci. Total Environ., 579, 657-666, https://doi.org/10.1016/j.scitotenv.2016.11.044, 2017.

Wang, C., Li, Y. Z., Tan, H., Zhang, A. K., Xie, Y. L., Wu, B., and Xu, H.: A novel microbe consortium, nano-visible light photocatalyst and microcapsule system to degrade PAHs, Chem. Eng. J., 359, 1065-1074, https://doi.org/10.1016/j.cej.2018.11.077, 2019.

Wang, C., Tan, H., Li, H., Xie, Y., Liu, H., Xu, F., and Xu, H.: Mechanism study of Chromium influenced soil remediated by an uptake-detoxification system using hyperaccumulator, resistant microbe consortium, and nano iron complex, Environ. Pollut., 257, 113558, https://doi.org/10.1016/j.envpol.2019.113558, 2020a.

Wang, C., Jia, Y., Li, J., Wang, Y., Niu, H., Qiu, H., Li, X., Fang, W., and Qiu, Z.: Effect of bioaugmentation on tetracyclines influenced chicken manure composting and antibiotics resistance, Sci. Total Environ., 867, 161457, https://doi.org/10.1016/j.scitotenv.2023.161457, 2023a.

Wang, C., Jia, Y., Li, J., Li, P., Wang, Y., Yan, F., Wu, M., Fang, W., Xu, F., and Qiu, Z.: Influence of microbial augmentation on contaminated manure composting: metal immobilization, matter transformation, and bacterial response, J. Hazard. Mater., 441, 129762, https://doi.org/10.1016/j.jhazmat.2022.129762, 2023b.

Wang, K., Jia, R., Li, L., Jiang, R., and Qu, D.: Community structure of *Anaeromyxobacter* in Fe(III) reducing enriched cultures of paddy soils, J. Soils Sed., 20, 1621-1631, https://doi.org/10.1007/s11368-019-02529-7, 2020b.

Wang, Q., Song, X., Wei, C., Jin, P., Chen, X., Tang, Z., Li, K., Ding, X., and Fu, H.: In situ remediation of Cr(VI) contaminated groundwater by ZVI-PRB and the corresponding indigenous microbial community responses: a field-scale study, Sci. Total Environ., 805, 150260, https://doi.org/10.1016/j.scitotenv.2021.150260, 2022.

Yaashikaa, P. R., Kumar, P. S., Jeevanantham, S., and Saravanan, R.: A review on bioremediation approach for heavy metal detoxification and accumulation in plants, Environ. Pollut., 301, 119035, https://doi.org/10.1016/j.envpol.2022.119035, 2022.

Yang, Y., Wang, H., Zheng, Y., Zhu, B., Wu, X., and Zhao, F.: Extracellular electron transfer of *Methylophilus methylotrophs*, Process Biochem., 94, 313-318, https://doi.org/10.1016/j.procbio.2020.05.001, 2020.

Yin, Y., Chen, Y., and Wang, J.: Co-fermentation of sewage sludge and algae and Fe^{2+} addition for enhancing hydrogen production, International Journal of Hydrogen Energy, 46, 8950-8960, https://doi.org/10.1016/j.ijhydene.2021.01.009, 2021.

Zhang, J., Liu, Y., Sun, Y., Wang, H., Cao, X., and Li, X.: Effect of soil type on heavy metals removal in bioelectrochemical system, Bioelectrochemistry, 136, 107596, https://doi.org/10.1016/j.bioelechem.2020.107596, 2020.

Zhang, Y., Zheng, S., Hao, Q., Wang, O., and Liu, F.: Respiratory electrogen *Geobacter* boosts hydrogen production efficiency of fermentative electrotroph *Clostridium pasteurianum*, Chem. Eng. J., 456, 141069, https://doi.org/10.1016/j.cej.2022.141069, 2023.

Zhang, Y., Shen, G., Hu, S., He, Y., Li, P., and Zhang, B.: Deciphering of antibiotic resistance genes (ARGs) and potential abiotic indicators for the emergence of ARGs in an interconnected lake-river-reservoir system, J. Hazard. Mater., 410, 124552, https://doi.org/10.1016/j.jhazmat.2020.124552, 2021.

Zhang, Y., Gu, A. Z., Cen, T., Li, X., He, M., Li, D., and Chen, J.: Sub-inhibitory concentrations of heavy metals facilitate the horizontal transfer of plasmid-mediated antibiotic resistance genes in water environment, Environ. Pollut., 237, 74-82, https://doi.org/10.1016/j.envpol.2018.01.032, 2018.

Zhu, J., Zhang, T., Zhu, N., Feng, C., Zhou, S., and Dahlgren, R. A.: Bioelectricity generation by wetland plant-sediment microbial fuel cells (P-SMFC) and effects on the transformation and mobility of arsenic and heavy metals in sediment, Environ. Geochem. Health, 41, 2157-2168, https://doi.org/10.1007/s10653-019-00266-x, 2019.

 Supplementary materials for

751 Cr(VI) reduction, electricity production, and microbial resistance variation in paddy soil under

752 microbial fuel cell operation

753 **Sections**

754 **Section 1:** Preparation of cathode supported by Fe_3O_4 catalyst

755 **Section 2:** Python code of Raspberry Pi voltage acquisition system

756 **Section 3:** Sampling method

757 **Section 4:** Soil DNA extraction method

758

759 **Table Captions**

760 **Table S1.** Main material dimensions

761 **Table S2.** Primer sequence of HRGs and MGEs

762 **Table S3.** Distribution percentage of EDS elements in electrode materials

763 **Table S4.** SMFC power generation performance on 15-day and 30-day

764 **Table S5.** Performance comparison of various configurations of SMFC.

765

766 **Figure captions**

767 **Fig. S1** SMFC structure and experimental grouping.

768 **Fig. S2** Electrode material characterization. (A, B) SEM images of GF without catalyst loading; (C, D)

769 SEM images of aluminum foam.

770 **Fig. S3** Variation of (A) total chromium and (B) Cr(VI) in overlying water during SMFC operation.

771   **Fig. S4** pH (A), EC (B) variation curves of soil.

772   **Fig. S5** Changes in soil enzyme activities during SMFC operation (A) Dehydrogenase (B) Urease (C)

773   Invertase (D) Acid Phosphatase.

774   **Fig. S6** Venn diagram on OTU level in different treatments.

775   **Fig. S7** Characterization of electrode materials before and after operation by EDS mapping. (A) EDS

776   image of cathode loaded with Fe_3O_4; (B) EDS image of cathode after the SMFC operation; (C) EDS

777   image of anode microorganisms; (D) EDS image of the anode after SMFC operation.

778

779   **Section 1:** Preparation of cathode supported by Fe_3O_4 catalyst

780   Cathode preparation: 100.00×50.00×3.00 mm graphite felt (GF) (purchased from Jiangsu Xinye

781   Electronic Materials Factory, Jiangsu, China) was selected as the cathode material of the SMFC, which

782   was ultrasonicated in ethanol for 50 min to remove impurities, removed, and washed. Then put it into an

783   oven and dried at 60℃ for 12 h. It was put into the hydrothermal synthesis reactor and added concentrated

784   nitric acid, and reacted at 90℃ for 9 h. After the reaction was completed, the GF was rinsed continuously

785   with ultrapure water to ensure that the pH of the rinsed water was neutral, and dried at 60℃ for 12 h to

786   complete the pre-activation of the GF. The Fe_3O_4 catalyst was obtained by dissolving 3.60 g of ferric

787   chloride hexahydrate, 6.00 g of sodium acetate, and 1.00 g of sodium citrate in 140 ml of ethylene glycol,

788   and repeatedly ultrasonicating for 2 h to form a homogeneous solution. The pre-activated GF was put

789   into a hydrothermal synthesis reactor: the Fe_3O_4 catalyst was added and soaked for half an hour and then

790   heated at 200℃ for 8 h. After heating, the reactor was cooled down to room temperature, washed

791   repeatedly with ultrapure water and ethanol, and then put into an oven at 60℃ to dry for 12 h. The

792   reaction was then dried at 60℃.

793

794 **Section 2:** Python code of Raspberry Pi voltage acquisition system

```python
1.  # -*- coding:UTF-8 -*-
2.  from threading import Timer
3.  import time
4.  import RPi.GPIO as GPIO
5.  import datetime
6.  import os
7.  import sys
8.  import xlwt
9.
10. sys.path.append('./modules/')
11.
12. from GetVoltage import get_voltage
13. from modules.ADS1263 import ADS1263
14.
15. GPIO.setmode(GPIO.BCM)
16. CollectTimes = 150
17.
18. def _get_average_list():
19.     """smooth"""
20.     if CollectTimes <= 0:
21.         print("Error number for the array to averaging!/n")
22.         return -1
23.     elif CollectTimes <= 5:
24.         return sum(VoltageArray) / CollectTimes
25.     else:
26.         return sum(VoltageArray) / CollectTimes
27.
28. # clean txt
29. book = xlwt.Workbook(encoding='utf-8',style_compression=0)
30. sheet = book.add_sheet('MFCdata',cell_overwrite_ok=True)
31. col = ('current time','MFC1','MFC2','MFC3')
32. for i in range(0,4):
33.     sheet.write(0,i,col[i])
34.
35. x=0
36. while(1):
37.     x=x+1
38.
39.     time.sleep(1)
```

```python
40.
41.     VoltageArray = []
42.     for i in range(CollectTimes):
43.         VoltageArray.append(get_voltage(0))
44.     adc1 = _get_average_list()
45.
46.     ###########################################################
47.
48.     VoltageArray = []
49.     for i in range(CollectTimes):
50.         VoltageArray.append(get_voltage(1))
51.     adc2 = _get_average_list()
52.
53.     ###########################################################
54.
55.     VoltageArray = []
56.     for i in range(CollectTimes):
57.         VoltageArray.append(get_voltage(2))
58.     adc3 = _get_average_list()
59.
60.     ###########################################################
61.
62.     curr_time = datetime.datetime.now()
63.     time_str = datetime.datetime.strftime(curr_time,'%Y-%m-%d %H:%M:%S')
64.
65.     datalist = [time_str,str(adc1),str(adc2),str(adc3 )]
66.     print(datalist)
67.
68.     for j in range(0, 4):
69.         sheet.write(x, j, datalist[j])
70.         savepath = '/home/pi/excel.xls'
71.         book.save(savepath)
72.
73.     time.sleep(598.5)
```

Section 3: Sampling method

We used a plastic cylindrical straw with a diameter of 0.40 cm and a length of 16.00 cm as the sediment sampler. The SMFC sediment part is inserted by the sampler vertically at a specific time, and then quickly removed, and the upper, middle, and lower parts of the sampler are mixed as a determination sample. And the fresh sample each time is only 8.00-16.00 g, only 0.20-0.40% of the SMFC. The total sampling amount shall not exceed 5% of the total population. Because the sampler is much smaller than SMFC, the disturbance is avoided to a great extent and the normal operation of SMFC is guaranteed.

Section 4: Soil DNA extraction method

Microbial DNA Rapid extraction kit (Shenggong Bioengineering Co., LTD., Shanghai, China) was used to extract total DNA from fresh samples. Specifically, 0.50 g sample, 0.50 g magnetic beads, and 1.00 ml SLX-Mlus Buffer were added in a 2.00 ml Eppendorf tube, and ground for 250 s under 45 HZ. Then added and mixed with 100 µl DS Buffer, and cultivated under 70 ℃ for 10 min and then 90℃ for 2 min. Then the mixture was centrifuged at 10000 g for 5 min at room temperature. 800 µl supernatant was moved to a new tube and added with 270 µl P2 buffer and 100 µl HTR reagent, and then cultivated under -20 ℃ for 5 min and then centrifuged again at 10000 g for 5 min. The supernatant was then moved to a new 2 ml tube added with the same amount of XP5 buffer and mixed upside down for 8 min. After magnetic rack adsorption, discard the residual liquid, remove the tube, add 500 µL XP5 Buffer, and mix well. Then adsorbed again with a magnetic rack, discard the residual liquid, remove the tube, add 500 µL PHB, and mix well. Then adsorbed again with a magnetic rack, discard the residual liquid, remove the tube, add 500 µL SPW Wash Buffer, and mix well (repeat this step twice). Then the mixture was adsorbed again with a magnetic rack, discard the residual liquid, was centrifuged in the tube under 10000

890   g for 10 s. Then the beads were adsorbed again with a magnetic rack, discard the residual liquid, and let

891   stand for 8 min. After that, the beads were added with 100 µL elution buffer, mixed, and let stand for 5

892   min. Finally, after adsorbing with a magnetic rack, the supernatant was moved to a new 1.00 ml

893   Eppendorf tube, and total DNA was obtained for further use. The PCR reaction system was constructed.

894

895   **Table S1** Main material dimensions

Material	Length/cm	Width/cm	Area/cm^2
Collector plate	10.50	5.50	57.75
Aluminum foam	6.60	5.40	35.64
GF	10.00	5.00	50.00

896

897   **Table S2** Primer sequence of HRGs and MGEs

Gene	Primer sequence	Function description	Ref
chrA-F	TCCTTCGGCGGCCCTGCCGGNCARATHGC	*chrA* encodes a transporter protein involved in chromate efflux.	(Rivera et al., 2008)
chrA-R	GTAGGTGGCCAGCTGCTNGCYTCNGGNCC		
chrB-F	CCGGAATTCATGCGTGTCTGGCGAACCCTGA	*chrB* genes regulate the transcription of genes in the transporter protein complex.	(Branco and Morais, 2013)
chrB-R	CCCAAGCTTTCACTCTGCGGAAGAACGA		

ChrR-F	AGGAACTTCTGCGTGCCCTC	The chromate reductase chrR is the best-known of the reductases that catalyze the reduction of Cr^{6+} to Cr^{3+}.	(Nepple et al., 2000; Baldiris et al., 2018).
ChrR-R	TACGGTGACAGTGCGTTTGC		
IntI-F	CGAACGAGTGGCGGAGGGTG		
IntI-R	TACCCGAGAGCTTGGCACCCA	MGEs such as integrons, plasmids, and transposons play a key role in the transfer of resistance genes between different microorganisms in the environment	(Wu et al., 2022; Wu et al., 2023).
tnpA02-F	GGGCGGGTCGATTGAAA		
tnpA02-R	GTGGGCGGGATCTGCTT		
tnpA05-F	GCCGCACTGTCGATTTTTATC		
tnpA05-R	GCGGGATCTGCCACTTCTT		

898

899

900

901

Table S3 Distribution percentage of EDS elements in electrode materials.

Elements	Samples					
	Cathode	Fe$_3$O$_4$-	Cathode	Anode	Anode with	Anode after

		cathode	after operation		EAB-loading	operation
C	93.74%	66.85%	33.83%	6.70%	14.65%	14.35%
O	6.26%	19.97%	38.96%	47.57%	18.49%	50.92%
Fe	n.d.	13.17%	8.07%	n.d.	n.d.	0.88
Mg	n.d.	n.d.	0.44%	n.d.	0.41%	n.d.
Al	n.d.	n.d.	3.34%	37.04%	53.72%	17.56%
Cr	n.d.	n.d.	0.08%	n.d.	n.d.	0.12%
Cu	n.d.	n.d.	n.d.	n.d.	1.59%	n.d.
Zn	n.d.	n.d.	n.d.	n.d.	1.81%	n.d.
Si	n.d.	n.d.	7.16%	8.68%	9.32%	2.58%
Na	n.d.	n.d.	2.18%	n.d.	n.d.	4.55%
Ca	n.d.	n.d.	4.81%	n.d.	n.d.	n.d.
K	n.d.	n.d.	1.12%	n.d.	n.d.	0.58%
Cl	n.d.	n.d.	n.d.	n.d.	n.d.	2.67%
P	n.d.	n.d.	n.d.	n.d.	n.d.	5.81%

902

903

Table S4 SMFC power generation performance on 15-day and 30-day

Resistor (Ω)	15d-Current density (mA/m^2)	15d-Power density (mW/m^2)	30d-Current density (mA/m^2)	30d-Power density (mW/m^2)
51	448.57	37.43	485.23	42.21
100	386.53	53.84	424.57	63.47
200	296.55	62.24	357.26	90.22
510	202.88	73.52	238.08	102.02
1000	131.18	60.60	157.54	87.35
2000	75.99	40.43	95.91	64.58

5100	31.55	17.77	43.88	34.41
10000	17.01	10.13	23.95	20.09

904 **Table S5** Performance comparison of various configurations of SMFC.

Reactor configuration	Chamber volume (L)	Output voltage(V)	Maximum power density (mW/m²)	Reference
Single-chamber SMFC	0.72	0.33	17.30	(Li et al., 2016)
Single-chamber SMFC	2.16	0.30	12.10	(Yu et al., 2017)
Two-chamber SMFC	4.20	0.40	29.78	(Srivastava et al., 2019)
Single-chamber circle SMFC	0.95	0.35	24.00	(Yu et al., 2021)
Single-chamber SMFC	8.00	0.40-0.60	0.20 mW	(Yoon et al., 2023)
Single-chamber circle SMFC	n.m.	n.m.	25.51	(Wang et al., 2023)
Single-chamber SMFC	9.70	n.m.	70.40±1.40	(Dhillon et al., 2023)
Two-chamber SMFC	0.05	n.m.	71.00 ± 0.82	(Zhang et al., 2023a)
Constructed wetland MFC	38.85	0.20	12.50	(Tao et al., 2023)
Constructed wetland MFC	4.08	0.43	28.10	(Niu et al., 2023)
Plant-SMFC	0.77	0.51	46.80	(V et al., 2023)
Single-chamber circle SMFC	2.00	0.17	10.00	(Youssef et al., 2023)
Constructed wetland MFC	2.70	0.39	4468.40	(Zhang et al., 2023b)

Two-chamber SMFC	0.50	0.31	20.35	(Zhang et al., 2024)
Constructed wetland MFC	13.00	0.17	1.40	(Dai et al., 2024)
Plant-SMFC	1.05	0.55	8957.70	(Chen et al., 2024)
Single-chamber circle SMFC	1.60	0.40	472.52±14.20	(Zhao et al., 2024)
Single-chamber circle SMFC	1.40	0.53	178.17	(Sun and Wang, 2024)
Single-chamber SMFC	2.30	0.75	102.00	This study

905

906

907
Fig. S1 SMFC structure and experimental grouping.
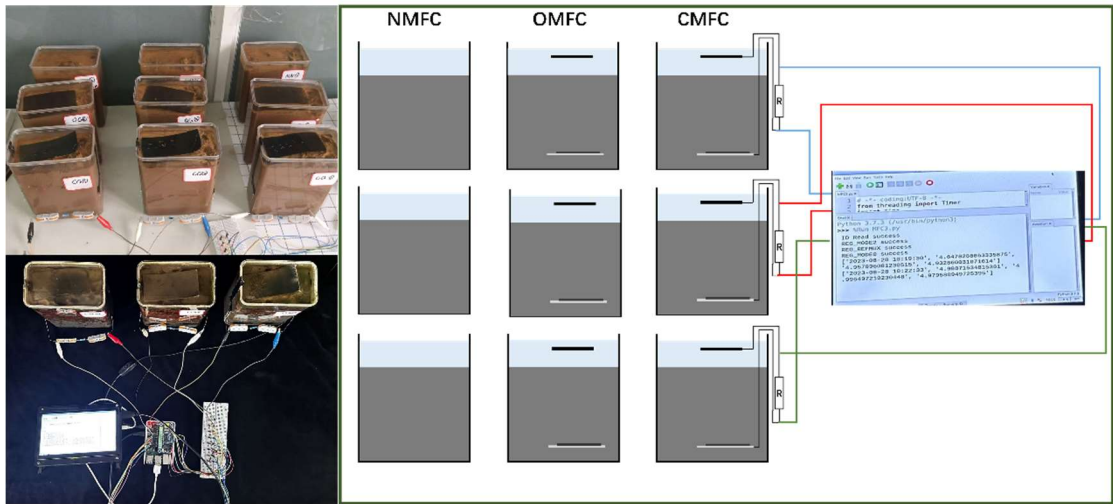
908 The left part of the picture is the SMFC photo, and the right part is the model groups. A plastic box

909 (140.00×85.00×165.00 mm) was used as the SMFC reactor, with 1.50 kg soil and overlying water of

910 3.00 cm to simulate the flooded state during rice planting. The cathode was floated on the water surface

911 while the anode was buried (about 3.00 cm from the bottom). The cathode and anode were connected to

912 a 2000 Ω resistor using titanium wire. The water level was kept constant by daily replenishment.

913

914   **Fig. S2** Electrode material characterization. (A, B) SEM images of GF without catalyst loading; (C,

915   D) SEM images of aluminum foam.

916

917

918   **Fig. S3** Variation of (A) total chromium and (B) Cr(VI) in overlying water during SMFC operation.

919

920   **Fig. S4** pH (A), EC (B) variation curves of soil.

921

922

923   **Fig. S5** Changes in soil enzyme activities during SMFC operation (A) Dehydrogenase (B) Urease (C)

924   Invertase(D) Acid Phosphatase.

925

926   **Fig. S6** Venn diagram on OTU level in different treatments

927

A

B

C

D

932   **Fig. S7** Characterization of electrode materials before and after operation by EDS mapping. (A) EDS

933   image of cathode loaded with Fe_3O_4; (B) EDS image of cathode after the SMFC operation; (C) EDS

934   image of anode microorganisms; (D) EDS image of the anode after SMFC operation.

935

936

937

938 **Reference:**
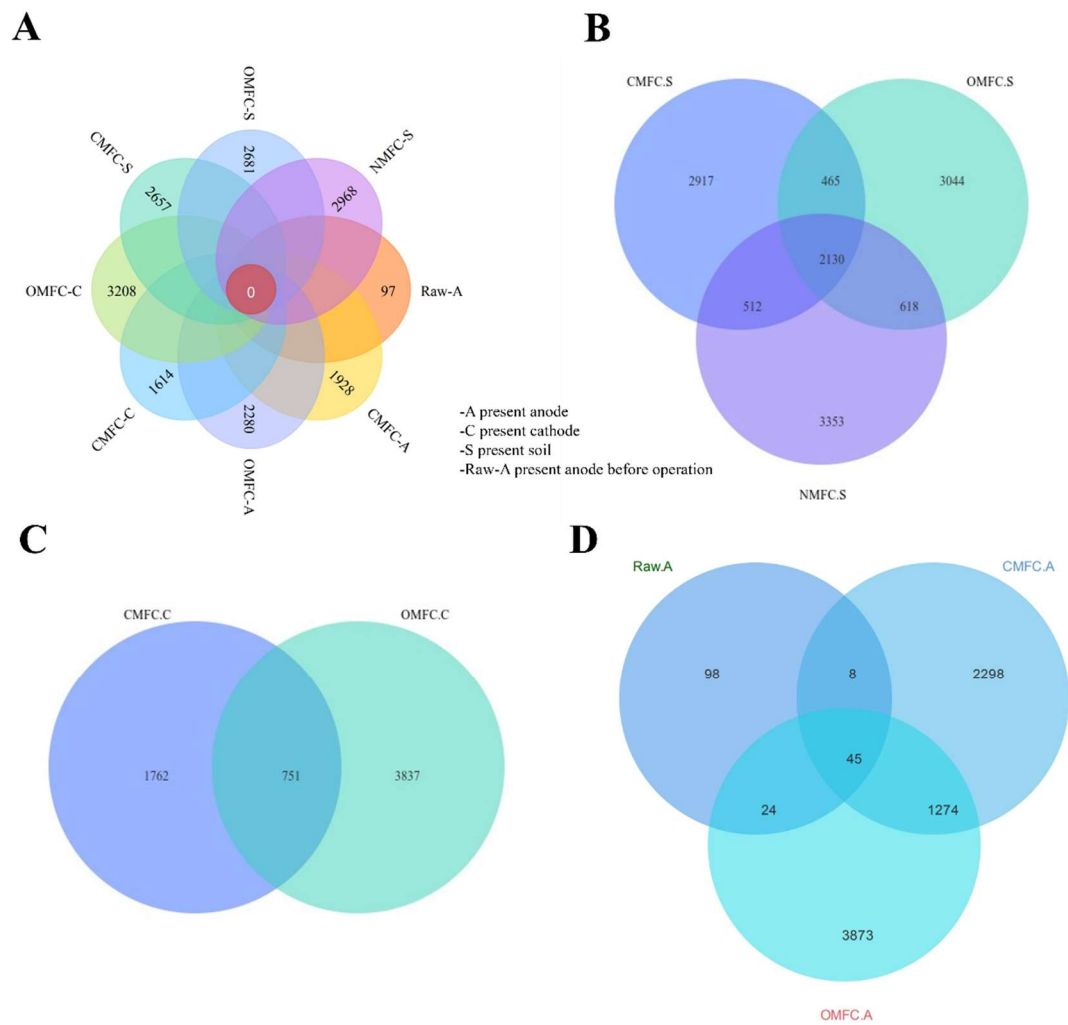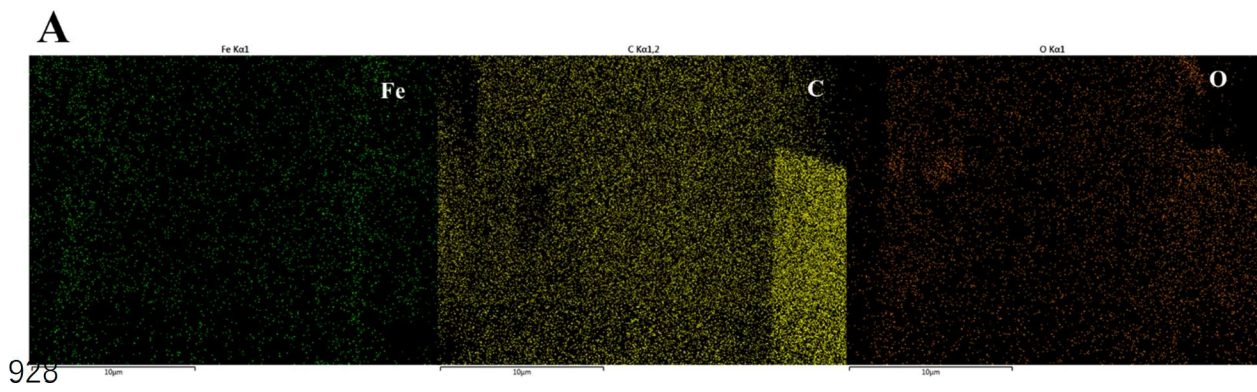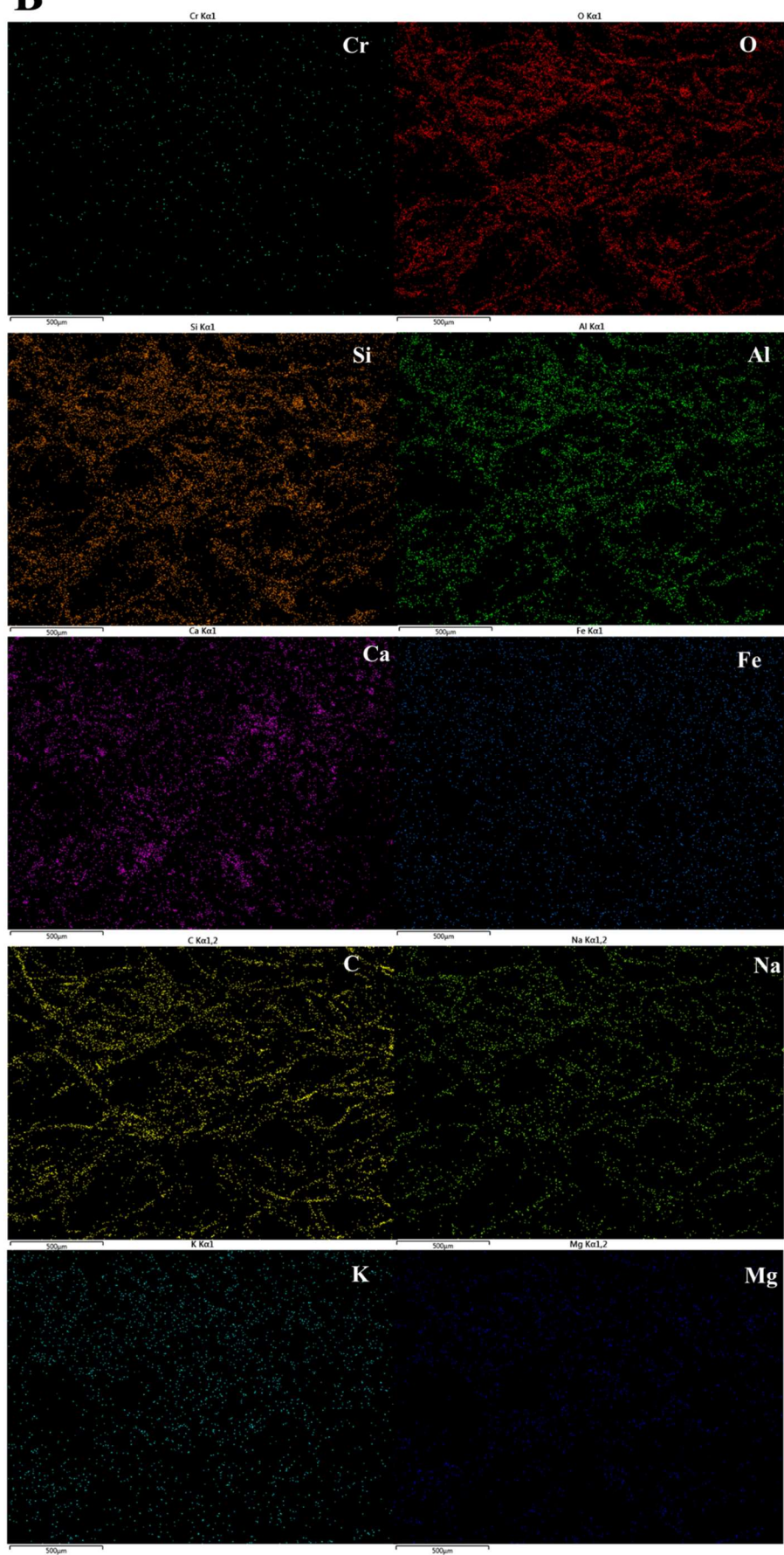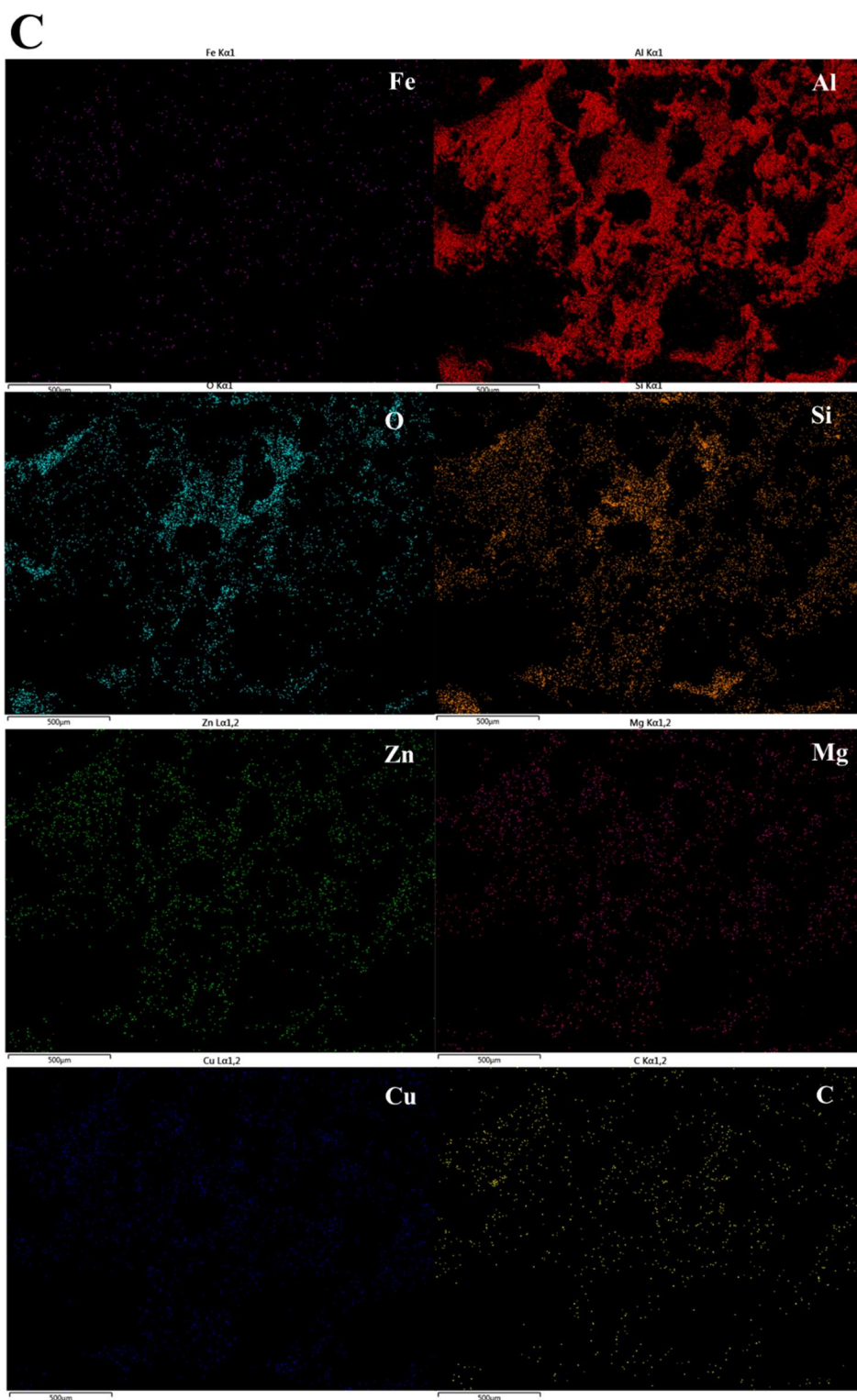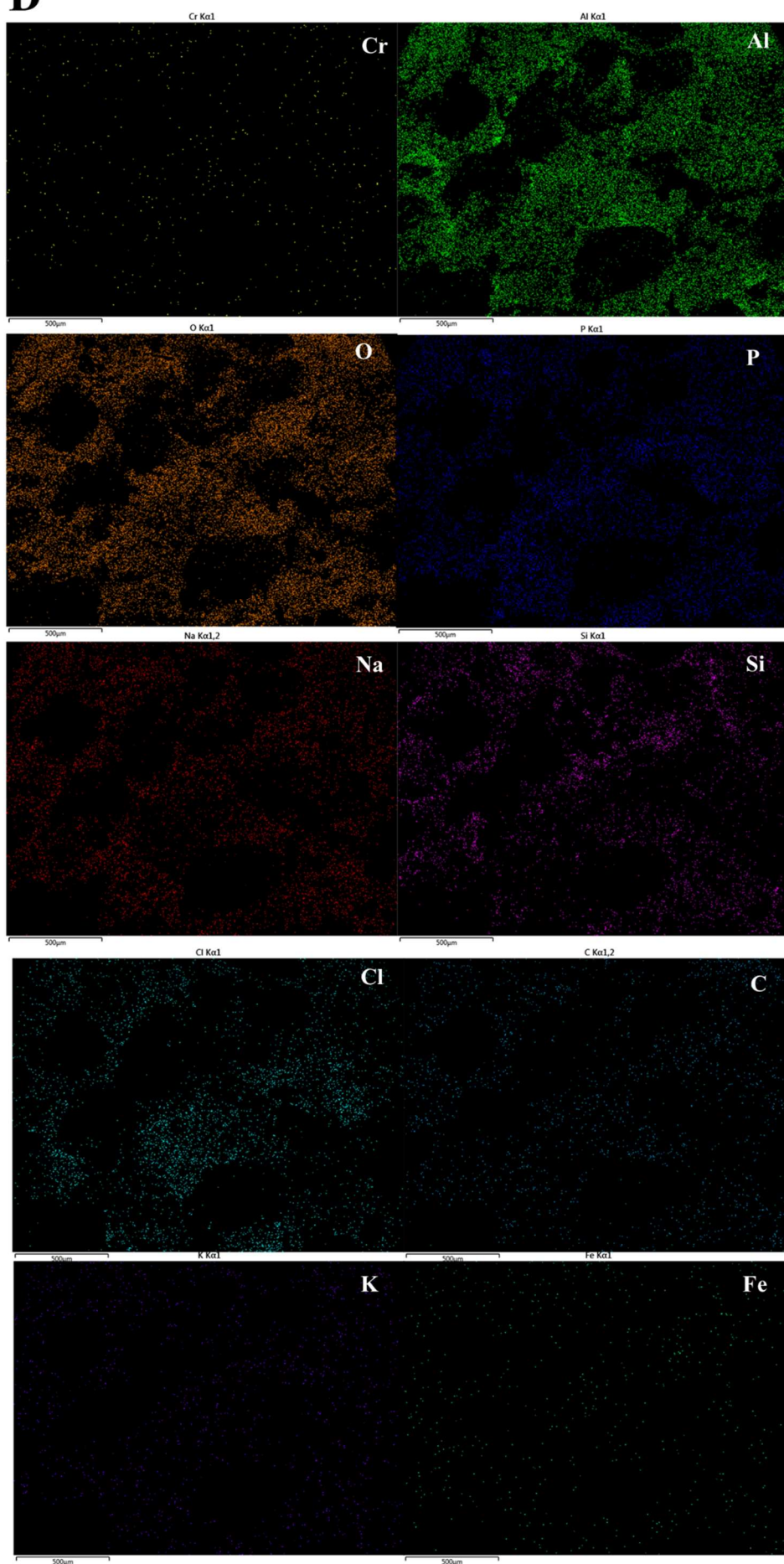
939 Baldiris, R., Acosta-Tapia, N., Montes, A., Hernández, J., and Vivas-Reyes, R.: Reduction of Hexavalent
940   Chromium and Detection of *Chromate Reductase* (*ChrR*) in *Stenotrophomonas maltophilia*,
941   Molecules, 23, 406, https://doi.org/10.3390/molecules23020406, 2018.

942 Branco, R. and Morais, P. V.: Identification and Characterization of the Transcriptional Regulator ChrB
943   in the Chromate Resistance Determinant of Ochrobactrum tritici 5bvl1, PLOS ONE, 8, e77987,
944   https://doi.org/10.1371/journal.pone.0077987, 2013.

945 Chen, B., Li, L., Cai, W., and Garg, A.: Bioelectricity generation in plant microbial fuel cells: Influence
946   of vegetation density and unsaturated soil properties, Biomass Bioenergy, 181, 107053,
947   https://doi.org/10.1016/j.biombioe.2024.107053, 2024.

948 Dai, M., Li, F., Zhang, J., Shi, Q., Wu, Y., and Kong, Q.: Treatment of formaldehyde-containing
949   wastewater and power generation by constructed wetland–microbial fuel cells enhanced by
950   formaldehyde-degrading bacteria, J. Water Process Eng., 59, 104984,
951   https://doi.org/10.1016/j.jwpe.2024.104984, 2024.

952 Dhillon, S. K., Dziegielowski, J., Kundu, P. P., and Di Lorenzo, M.: Functionalised graphite felt anodes
953   for enhanced power generation in membrane-less soil microbial fuel cells, RSC Sustainability,
954   1, 310-325, https://doi.org/10.1039/D2SU00079B, 2023.

955 Li, X., Wang, X., Zhao, Q., Wan, L., Li, Y., and Zhou, Q.: Carbon fiber enhanced bioelectricity generation
956   in soil microbial fuel cells, Biosensors Bioelectron., 85, 135-141,
957   https://doi.org/10.1016/j.bios.2016.05.001, 2016.

958 Nepple, B. B., Kessi, J., and Bachofen, R.: Chromate reduction by *Rhodobacter sphaeroides*, J. Ind.
959   Microbiol. Biotechnol., 25, 198-203, https://doi.org/10.1038/sj.jim.7000049, 2000.

960 Niu, Y., Qu, M., Du, J., Wang, X., Yuan, S., Zhang, L., Zhao, J., Jin, B., Wu, H., Wu, S., Cao, X., and
961   Pang, L.: Effects of multiple key factors on the performance of petroleum coke-based
962   constructed wetland-microbial fuel cell, Chemosphere, 315, 137780,
963   https://doi.org/10.1016/j.chemosphere.2023.137780, 2023.

964 Rivera, S. L., Vargas, E., Ramírez-Díaz, M. I., Campos-García, J., and Cervantes, C.: Genes related to
965   chromate resistance by *Pseudomonas aeruginosa PAO1*, Antonie Van Leeuwenhoek, 94, 299-
966   305, https://doi.org/10.1007/s10482-008-9247-x, 2008.

967 Srivastava, P., Gupta, S., Garaniya, V., Abbassi, R., and Yadav, A. K.: Up to 399 mV bioelectricity
968   generated by a rice paddy-planted microbial fuel cell assisted with a blue-green algal cathode,
969   Environ. Chem. Lett., 17, 1045-1051, https://doi.org/10.1007/s10311-018-00824-2, 2019.

970 Sun, M. and Wang, C.: The application of ferrous and graphitic N modified graphene-based composite
971   cathode material in the bio-electro-Fenton system driven by sediment microbial fuel cells to
972   degrade methyl orange, Heliyon, 10, e24772, https://doi.org/10.1016/j.heliyon.2024.e24772,
973   2024.

974 Tao, M., Kong, Y., Jing, Z., Guan, L., Jia, Q., Shen, Y., Hu, M., and Li, Y.-Y.: Acorus calamus recycled
975   as an additional carbon source in a microbial fuel cell-constructed wetland for enhanced nitrogen
976   removal, Bioresour. Technol., 384, 129324, https://doi.org/10.1016/j.biortech.2023.129324,
977   2023.

978 V, K. K., K, M. m., Manju, P., and Gajalakshmi, S.: Harnessing plant microbial fuel cells for resource

979   recovery and methane emission reduction in paddy cultivation, Environ. Chem. Lett., 294,
980   117545, https://doi.org/10.1016/j.enconman.2023.117545, 2023.

981 Wang, H., Long, X., Cao, X., Li, L., Zhang, J., Zhao, Y., Wang, D., Wang, Z., Meng, H., Dong, W., Jiang,
982   C., Li, J., and Li, X.: Stimulation of atrazine degradation by activated carbon and cathodic effect
983   in   soil   microbial   fuel   cell,   Chemosphere,   320,   138087,
984   https://doi.org/10.1016/j.chemosphere.2023.138087, 2023.

985 Wu, C., Song, X., Wang, D., Ma, Y., Ren, X., Hu, H., Shan, Y., Ma, X., Cui, J., and Ma, Y.: Effects of
986   long-term microplastic pollution on soil heavy metals and metal resistance genes: Distribution
987   patterns   and   synergistic   effects,   Ecotoxicol.   Environ.   Saf.,   262,   115180,
988   https://doi.org/10.1016/j.ecoenv.2023.115180, 2023.

989 Wu, Y., Wen, Q., Chen, Z., Fu, Q., and Bao, H.: Response of antibiotic resistance to the co-exposure of
990   sulfamethoxazole and copper during swine manure composting, Sci. Total Environ., 805,
991   150086, https://doi.org/10.1016/j.scitotenv.2021.150086, 2022.

992 Yoon, Y., Kim, B., and Cho, M.: Mineral transformation of poorly crystalline ferrihydrite to hematite and
993   goethite facilitated by an acclimated microbial consortium in electrodes of soil microbial fuel
994   cells, Sci. Total Environ., 902, 166414, https://doi.org/10.1016/j.scitotenv.2023.166414, 2023.

995 Youssef, Y. A., Abuarab, M. E., Mahrous, A., and Mahmoud, M.: Enhanced degradation of ibuprofen in
996   an integrated constructed wetland-microbial fuel cell: treatment efficiency, electrochemical
997   characterization, and microbial community dynamics, RSC Advances, 13, 29809-29818,
998   https://doi.org/10.1039/D3RA05729A, 2023.

999 Yu, B., Tian, J., and Feng, L.: Remediation of PAH polluted soils using a soil microbial fuel cell:
1000   Influence of electrode interval and role of microbial community, J. Hazard. Mater., 336, 110-
1001   118, https://doi.org/10.1016/j.jhazmat.2017.04.066, 2017.

1002 Yu, B., Feng, L., He, Y., Yang, L., and Xun, Y.: Effects of anode materials on the performance and anode
1003   microbial community of soil microbial fuel cell, J. Hazard. Mater., 401, 123394,
1004   https://doi.org/10.1016/j.jhazmat.2020.123394, 2021.

1005 Zhang, C., Lu, H., Wang, B., and Hu, Z.: Study on the Performance of Two-Compartment Microbial Fuel
1006   Cells Under Different Heavy Metal Concentrations, Water, Air, Soil Pollut., 235, 58,
1007   https://doi.org/10.1007/s11270-023-06869-6, 2024.

1008 Zhang, G., Wang, Z., Liu, M., Huang, L., Jiao, Y., and Zhao, Z.: Self-Driven Electrokinetic Remediation
1009   of Cd Contamination Soil by Using Double-Chamber Microbial Fuel Cell, J. Electrochem. Soc.,
1010   170, 075502, https://doi.org/10.1149/1945-7111/ace6fd, 2023a.

1011 Zhang, Q., Wang, L., Xu, D., Tao, Z., Li, J., Chen, Y., Cheng, Z., Tang, X., and Wang, S.: Accelerated
1012   Pb(II) removal and concurrent bioelectricity production via constructed wetland-microbial fuel
1013   cell: Structural orthogonal optimization and microbial response mechanism, J. Water Process
1014   Eng., 56, 104287, https://doi.org/10.1016/j.jwpe.2023.104287, 2023b.

1015 Zhao, S., Li, H., Zhou, J., Sumpradit, T., Salama, E.-S., Li, X., and Qu, J.: Simultaneous degradation of
1016   NSAIDs in aqueous and sludge stages by an electron-Fenton system derived from sediment
1017   microbial fuel cell based on a novel Fe@Mn biochar GDC, Chem. Eng. J., 482, 148979,
1018   https://doi.org/10.1016/j.cej.2024.148979, 2024.

1019

1020

1021